NTNU
Norwegian University of
Science and Technology

Catalytic combustion of methane over nickel cobalt based catalysts derived from hydrotalcite precursors.

Leyman Maleki Bakali-Hemou

Master's Thesis
Submission date: June 2017
Supervisor: De Chen, IKP

Norwegian University of Science and Technology
Department of Chemical Engineering

Année 2016-17

MASTER DE CHIMIE DE PARIS CENTRE

Spécialité : Matériaux

Rapport de stage 5C101

Catalytic combustion of methane over nickel cobalt based catalysts derived from hydrotalcite precursors.

Leyman Maleki Bakali-Hemou

De Chen, Professeur

Catalysis group, Department of Chemical Engineering, Norwegian University of Science and Technology (NTNU), Trondheim, NORVEGE

PREFACE

This master thesis was performed as “stage de master” for the master diploma in Chemistry specialization Chemistry and Physical-Chemistry of Materials of the French university Université Pierre et Marie Curie (UPMC-Paris 6, France). Therefore, the organisation of this thesis is based on my home university regulation and all the planned experiments could not be performed as my period in NTNU was limited and could not be extended (which can be observed in the data collected). However, I would like to thanks Pr. Corinne Chaneac (Head of the Master of chemistry and physical chemistry of materials in UPMC) for allowing me to perform this master thesis in Norway and Mme Tourte (social worker in UPMC) for helping me during my studies, I’m really grateful for everything.

I would like to thanks Pr. De Chen for this master thesis subject, Dr. Kumar Ranjan Rout and future Dr. Shirley Liland for the guidance and patience (Shirley you always found a solution to all the problems I faced during the thesis). Then, I would like to thanks the engineers Karin, Harry, Magnus and Sergey (department of materials technology) for the trainings and help with the apparatus. I also thank all the master students performing their master thesis with me: Raghnild, Stine, Signe, Moses, Petter, Sebastian, Bjorn, Nick, Matus, Jianyu. Moments with you were so fun and I hope we can meet again. Finally I would like to express my deep thanks to Nnamdi Ubabuike for keeping my Chinemerem during my period in Trondheim and for being a support in hard and stressing periods (even if you also stressed me a lot!). This period in Trondheim was wonderful thanks to all the incredible people I met here (Knut, Mary, Sture, Imran, Emelda, my roommates…). I don’t regret the semester I have spent here.

I hereby declare that this is an independent work according to the exam regulations of the Norwegian university of Science and Technology.

Trondheim, 20/06/2017.

Leyman Maleki BAKALI-HEMOU

Table of Contents

ABSTRACT

This master thesis dealt with the combustion of methane over Ni-Co catalysts with different Ni:Co ratio in order to achieve total conversion. Thus, these mixed oxide catalysts derived from hydrotalcite precursors were investigated for this purpose in order to determine the kinetic of this oxidative reaction. The 5wt% metal loading catalysts were prepared by co-precipitation method and calcined at 600°C. Their textural properties were analysed by X-ray diffraction (XRD), X-ray fluorescence spectroscopy (XRF), Scanning electron microscopy coupled with X-ray energy dispersive spectroscopy (SEM-XEDS), N_2 adsorption-desorption. The 12, 20, 30 and 40wt% metal loading catalysts were prepared and characterized by the former master student Bilal Yousaf. The characteristics of these catalysts agreed with the properties of mixed oxide derived from hydrotalcites described in the literature. Indeed, these mixed oxides display larger surface areas than their hydrotalcite precursors and contain spinel phases. However, their composition shows that a small amount of magnesium is lost during the synthesis and the samples contain a non negligible amount of zinc and copper.

The methane oxidation over these catalysts was performed in a fixed bed reactor and followed by gas chromatography (GC). The methane conversion versus the furnace temperature was calculated based on the integrated peaks of the chromatograms. Evolution of the catalysts during the reduction and combustion steps was followed by Ultraviolet-Visible spectroscopy. This technique enabled to observe the two transitions in the cobalt reduction namely Co^{3+} to Co^{2+} and Co^{2+} to Co^{0}. Furthermore, it also shows that the methane conversion is related to the oxidation of the active phase as oxidized surfaces are required in order to achieve high conversion. Then, it is assumed that cobalt is not totally oxidized during the combustion of methane but forms CoO. Moreover, it was observed a modification in the colour for some bimetallic catalysts which became blue for the 12wt% catalysts and purple for the 5wt% catalysts at the end of the tests. These blue/purple particles are assumed to be sintering CoO with Al_2O_3 forming $CoAl_2O_4$. Finally, the reflectance curves and the methane conversion show an oscillation in the methane conversion over some low loading bimetallic Ni-Co catalysts. Besides, production of carbon monoxide at high temperatures is also observed. Therefore, assumptions according to the literature to explain these observations are a cyclic oxidation/reduction and/or a deactivation (and recovery) of the catalyst by sintering and coke. To conclude, these phenomena occurring during the methane combustion over these Ni-Co catalysts should be understood before calculating the kinetic of this oxidative reaction with accuracy.

1. INTRODUCTION

Methane, the main constituent of natural gas, is the most abundant source of hydrocarbon on earth. Therefore, it has received attention as potential substitute to oil, for instance in the automobile industry with the development of natural gas vehicles (NGV)[8, 43, 44]. Indeed, methane is considered as a clean fuel because of its high-energy production combine with reduction of NO_x emission, which is the main cause of photochemical smog[43]. Moreover, methane is also used in the chemical industry for the production of synthesis gas. Indeed, steam methane reforming is the main industrial process for hydrogen and synthesis gas production[1] (almost fifty percent of the worldwide production). The conversion of this gas is carried out in a conventional reactor followed by Water-gas shift reactor and equipment for hydrogen separation and purification. Nevertheless, harsh operating conditions in the conventional reactor, namely gas pressure from 14 to 20 bar and temperature from 800°C to 1000°C, over catalysts are required in order to obtain high methane conversion. However, these conditions favour deactivation of the catalysts by carbon deposition[42]. Thus, to reduce the high-energy requirement of this process and enhance the catalyst stability, a promising alternative is the development of a compact multichannel reformer[16, 19,46]. In this system, the highly exothermic catalytic combustion of methane is integrated to the steam reforming process in adjacent channels in order to provide the required heat for methane conversion to hydrogen. Indeed, the catalytic combustion of hydrocarbon fuels has been intensively studied as an environmental friendly way to produce thermal energy because of its high efficiency and low emission of unburnt methane compared to conventional flame-combustion system[2]. Indeed, methane is 21times higher greenhouse gas than carbon dioxide. Therefore, reducing exhausted emission of unburnt methane has become a big issue and the catalytic combustion is mainly investigated in order to achieve total oxidation of methane at low temperature. The nickel cobalt mixed oxide based catalysts are investigated for this compact reformer. Indeed, they exhibit good performance on both catalytic combustion and steam reforming of methane depending on the Ni/Co ratios[8,11,45]. Therefore, this master thesis deals with the catalytic combustion of methane over nickel cobalt mixed oxide catalysts derived from hydrotalcite like precursors with different Ni/Co ratio, in order to determine the kinetic of this oxidative reaction.

2. STATE OF THE ART

2.1 Combustion and catalytic combustion

Hydrocarbon combustion has been studied for heat production and unburnt fuel removal[2]. The production of energy by methane combustion or natural gas is well-established[3] and represented by the equation [2.1].

$$CH_4 + 2O_2 = CO_2 + H_2O \quad \Delta H°_{298K} = -802.7\ kJ/mol \qquad [2.1]$$

Nevertheless, this overall equation is a gross simplification with the actual mechanism, which involves many free radical chain reactions. Furthermore, the gas-phase combustion can only occur within given flammability limits and the temperature can rapidly rise above 1600°C, which favours direct combination of nitrogen and oxygen to unwanted nitrogen oxides NOx[4]. Therefore, catalytic combustion, which is an oxidative reaction of the hydrocarbon fuel by using solid catalysts, gives the possibility to control the reaction conditions and temperature[2,4]. These enable to minimize emission of NOx and CO, coke formation, catalyst sintering and permit to work at lower temperature[2,4,5]. Indeed, catalytic combustion is generally classified into three categories according to the temperature zones of the combustion system[2]. Low-temperature combustion is operated below 300°C, the intermediate-temperature combustion from 300°C to 800°C and the high-temperature combustion above 800°C. The catalytic oxidation of methane produces carbon monoxide via partial oxidation route or carbon dioxide via total combustion route depending on the methane to air ratio. Other reactions may be involved to a greater or less extent including steam reforming, water gas shift and reverse methanation[4] (see equations below).

Methane steam reforming:

$$CH_4 + H_2O = CO + 3H_2, \qquad \Delta H°_{298K} = +206.1\ kJ/mol$$

Water gas-shift:

$$CO + H_2O = CO_2 + H_2, \qquad \Delta H°_{298K} = -41\ kJ/mol$$

Reverse methanation

$$CH_4 + 2H_2O = CO_2 + 4H_2 \qquad \Delta H°_{298K} = +164\ kJ/mol$$

However, methane oxidation is complicated because it is necessary to initiate the reaction at quite high temperature, compared to natural gas which contains higher hydrocarbon so a

lower light-off temperature[4]. Therefore, complete combustion of methane is known to be difficult to achieve so requires very active catalysts. To summarize, the literature shows that the catalytic combustion of methane strongly depends on the:

- Oxygen to methane ratio: Because under oxygen deficient atmosphere only carbon monoxide is formed while under oxygen, rich condition carbon dioxide is observed.
- Catalyst activity: this depends on the nature of support, metal loading, particle size, thermic treatment[4], etc.

2.2 Catalysts for methane combustion

2.2.1 Active phases for methane combustion

Literature presents various catalysts for methane total oxidation. Noble metal based catalysts, especially containing palladium or platinum exhibit excellent performances on catalytic combustion of methane at low temperature[2, 3, 4, 5]. Lee and al[4] claimed that Pd based catalyst has been found to be the most efficient for catalytic oxidation of methane to carbon dioxide and water. However, the low abundancy and high price of these metals limit the commercial applications of these catalysts. Therefore, transition metal oxides are studied as substitutes of these noble metals even though they display lower intrinsic activity on the methane oxidation. In fact, recent studies have focused on the enhancement of transition metal oxide catalysts in order to reach the activity of noble metals. Thus, cobalt has been intensively studied as active metal in complete oxidation of methane. Indeed, Co_3O_4 based catalysts are well-known for being very active in this reaction[2, 4, 6]. For instance, Li Z. H. and al[7] reported that Pd/Co_3O_4 exhibit higher activity than Pd/Al_2O_3. Even though, nickel oxide displays a lower activity in catalytic combustion than cobalt oxide Co_3O_4, Lim and al[8] demonstrated that a suitable mixing of NiO and Co_3O_4 phases achieves superior activity for methane oxidation. In fact, mixed oxide catalysts are attractive because of their low cost and abundant resource. Studies showed that specific crystal structures of mixed oxides such as perovskite, spinel and hexaaluminate are active for oxidation of hydrocarbons[2]. This is the case of Co_3O_4 which crystallize in spinel structure, perovskite based metal oxide catalysts $La_{1-x}A_xMnO_3$ (A= Sr, Eu, Ce) also display complete oxidation of methane at temperature between 500-600°C[9, 10]. The major feature of these mixed oxide materials, is the possibility to control the oxidation activity by appropriate selection of components and composition without a modification in the crystal structure. Thus, different studies demonstrated that Ni-Co mixed oxides exhibit better

catalytic activity on methane combustion than pure NiO and Co_3O_4 due to a close relationship between structure and physical properties[8]. The Ni-Co mixed oxide catalysts prepared during this master thesis are derived from hydrotalcite materials.

2.2.2 Hydrotalcite like compounds

The hydrotalcite mineral discovered in Sweden around 1842 is a hydroxycarbonate of magnesium and aluminium with the formula $Mg_6Al_2(OH)_6CO_3.4H_2O$. It belongs to the class of anionic clays so presents a hydrated lamellar structure. The structure of this material is described as a brucite $Mg(OH)_2$ in which some Mg^{2+} ions are substituted by trivalent ions (Al^{3+}, Fe^{3+}, etc.) generating positive charges which are compensated by CO_3^{2-} ions. In details, a brucite $Mg(OH)_2$ is formed of Mg^{2+} octahedra coordinated to OH^- (hydroxo bridges) linked by the edges forming infinite sheets. These octahedral sheets are stacked on top of each other and held together by hydrogen bonds. When a Mg^{2+} ion is substituted by an Al^{3+} ion for instance, it creates a positive charge on a octahedra sheet which is compensated by a CO_3^{2-} anion which is located in the interface of two brucite sheets. Therefore, interlayers constituting the hydrotalcite structure contain carbonate ions and water of crystallization[11].

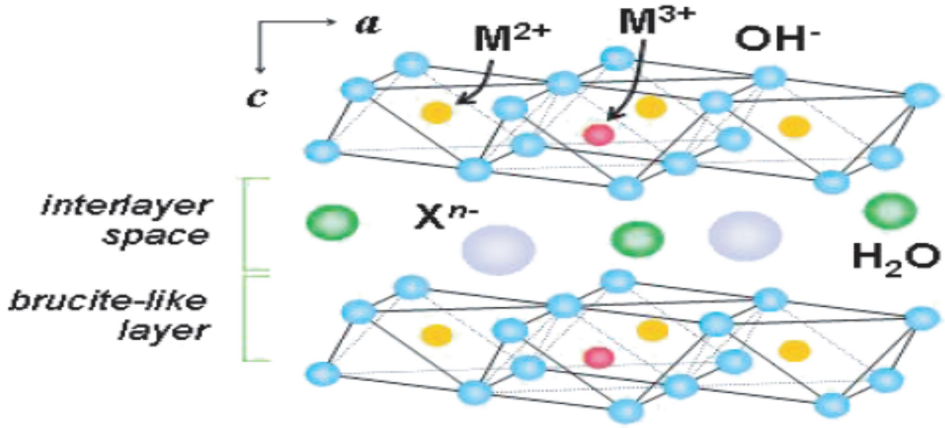

Fig. 1.1: Schematic illustration of the structure of hydrotalcite like compounds[29] .

Hydrotalcite like compounds are composed of other cations and anions than the natural minerals. Their general formula is described below, where M(II) represent cationic ions charged +2, M(III) ion charged +3 and A^{n-} is the compensator anion.

$$[M(II)_{1-x}\, M(III)_x(OH)_2]^x \left(A_{\frac{x}{n}}^{n-}\right) mH_2O$$

Hydrotalcite like compounds are mainly used after calcination when transformed to mixed oxides. Indeed, these mixed oxides derived from a hydrotalcite structure exhibit high surface

areas and dispersion of active sites, basic properties and good thermal stability[11, 12]. Therefore, this class of materials have been applied in different processes related to heterogeneous catalysis, as support and catalyst for hydrogenation and reforming. For instance, Khassin[13] and Chmielarz[14] respectively reported that mixed oxide catalysts derived from hydrotalcites containing cobalt show excellent activity on Fischer-Tropsch synthesis and catalytic removal of NOx[15]. Moreover, the hydrotalcite structure permits to highly disperse and stabilize active metals such as cobalt in its oxide matrixes composed of magnesium and aluminium with just slight phase separation during calcination or high temperature application[12]. Indeed, it has been reported that at high temperature spinel phase Co_3O_4 is decomposed to less active CoO compound[2, 5, 12]. Therefore, mixed oxides derived from hydrotalcite compounds show a great potential for catalytic combustion reactions[5, 8, 12].

2.3 Compact multichannel reformer

Coupling of strong endothermic reactions with heat exchange in a multifunctional reactor is often found in large-scale processes such as hydrocarbon cracking, steam reforming and dehydrogenation. Indeed, a heating medium or an exothermic reaction can provide the heat demand of an endothermic reaction at high temperature. According to Zanfir and al[16] there are three ways to combine the endothermic process and the heat supplier namely *in situ*, *chronologically segregated* and *spatially segregated* heat generation[17]. During in situ heat generation, reactants for both exothermic and endothermic reactions are mixed together and all reactions run in parallel, subject to a direct heat transfer within the reaction mixture. This method has been industrially applied in secondary methane reforming within ammonia synthesis[18] and hydrogen cyanide production[17] in which hydrogen combustion is used as the in situ heat generator. During the *chronologically segregation (*also called regenerative heat exchange) the catalyst fixed bed is heated by the exothermic reaction cycle and the store heat is consumed in the next cycle when the endothermic process takes place, cooling the fixed bed. Finally, the spatially segregation provides the heat for the endothermic reaction is indirectly transferred by the combustion process through heat exchanger. These three alternatives mentioned above have been investigated for the steam methane reforming coupled with methane catalytic combustion[16]. However, in situ process requires bifunctional catalysts that promote both exothermic and endothermic reactions in the same temperature range. Moreover, hot spots can occur in a chronologically segregated way, which may damage the catalyst and the reactor materials. Therefore, development of compact channel reformers is mainly based on spatially segregation heat generation.

A compact multichannel reformer is a reactor that combines three process steps: the combustion, the heat recovery and the reforming reaction into a tubular module[19]. Indeed, the catalytic combustion of a light hydrocarbon (methane or hydrogen) is integrated to a channel Fig 1.2 or more Fig 1.3 of the reactor in order to directly provide the heat required for the reforming reaction. Therefore, this system, generally designed as a multiple catalyst-coated channels in a plate or monolithic reactor, is studied for the refinery scale hydrogen production to reduce the energetic cost. Moreover, the development of this small reactor enables the placement of the hydrogen generation unit near the point of use[16]. However, this system can present some drawbacks that need to be taken into consideration. For instance, the high temperature generated in the combustion duct can lead to a decrease of the catalyst stability, a heat loss due to hot spots, and a possible explosion of the combustor[19].

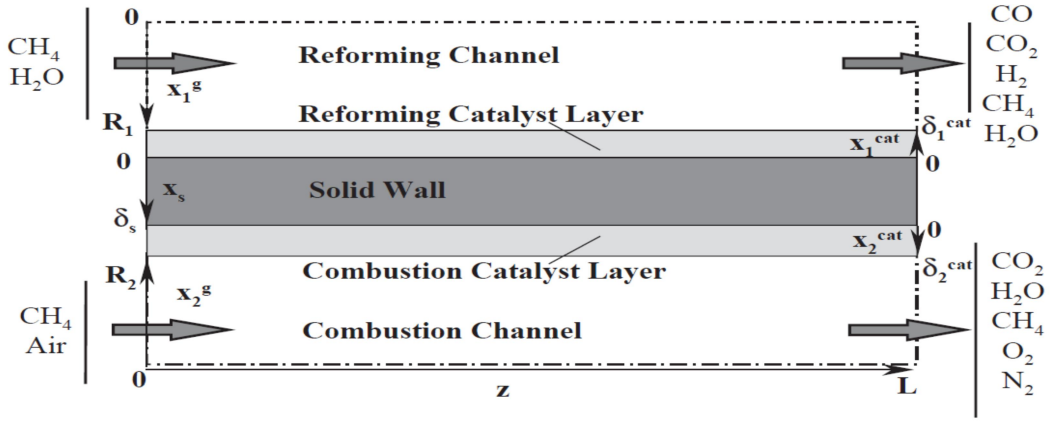

Fig. 1.2: Schematic illustration of a two channel compact reformer developed by Zanfir and al[16]. The combustion and reforming channels are separated by a solid wall constituting of catalyst layers.

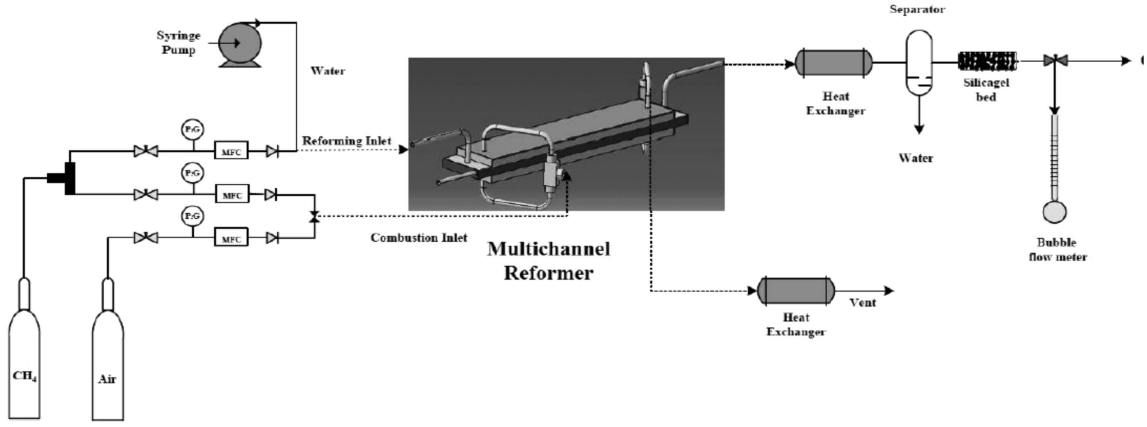

Fig. 1.3: Schematic illustration of a multichannel compact methane reformer developed by Irankha and al[19]. The combustion channels are located from either side of the methane reforming channel.

3 MATERIALS AND METHODS

3.1 Synthesis of the nickel cobalt mixed oxides catalysts

The nickel cobalt mixed oxides derived from hydrotalcite precursors are prepared by co-precipitation method[11, 28]. According to Cavani and al[11] the first requirement in order to obtain a hydrotalcite like compound is to choose the correct ratio of cations and anions because in the final component these values must be:

$$0.2 \leq \frac{M(II)}{M(II)+M(III)} \leq 0.4$$

$$\frac{1}{n} \leq \frac{A^{n-}}{M(III)} \leq 1$$

$M(II)$: Molar quantity of M^{2+}cations, $M(III)$: molar quantity of M^{3+}cations and A^{n-}: molar quantity of the anions in the interlayer

Following these requirement, calculations in order to prepare and determine the general formula of the nickel cobalt hydrotalcite like catalysts are explained in the Appendix A. The procedure in order to prepare the mixed oxide compound the bimetallic mixed oxide catalyst with a total nickel cobalt metal loading of 5 wt% (2,5wt% Ni and 2,5wt% Co) derived from $[Ni_{0.15}\ Co_{0.15}Mg_{5.7}\ Al_2\ (OH)_{16}]^{2+}.(CO_3^{2-}).mH_2O$ hydrotalcite is explained as followed:

The cation precursors: $Mg(NO_3)_2.6H_2O$ (54,83g, Sigma-Aldrich, purity >99%), $Al(NO_3)_3.9H_2O$ (28,13g, Sigma-Aldrich, purity >98%), $Ni(NO_3)_2.6H_2O$ (1,62g, Sigma-Aldrich, purity 99,999%) and $Co(NO_3)_2.6H_2O$ (1,62g, ACROS ORGANICS purity >99%) were dissolved in 400ml distilled water, then added into a three-neck round bottom flask with a stirring and a condenser. The anion precursors NaOH (24g, MERCK purity >98%) and Na_2CO_3 (5,97g, VWR chemicals purity 100%) were dissolved in 400ml distilled water and fed into the three-neck round bottom flask droplet by droplet within more or less 2h. After complete addition of the alkaline solution, the pH of the mixture is adjusted to a value comprise between 8 to 9, by adding droplets of HNO_3 60% or NaOH solution. The mixture was kept under stirring at 80°C for 16h. The precipitate obtained was cooled, filtrated, washed with at least 1.6L of distilled water and dried at 70°C for 10h. The mixed oxide catalyst is obtained by calcination of the precipitate at 600°C for 6h using a heating rate of 5°C/min.

3.2 Characterization of the catalysts

3.2.1 X-ray diffraction (XRD)

A crystalline material is defined by regular, repeating planes of atoms (crystal lattice) in the three direction of space. When an incident X-ray beam (electromagnetic radiation) is directed at a sample of this material under an angle θ, it interacts with electrons of the planes of atoms. Thus, parts of the beam are reflected, transmitted, refracted, and scattered by the crystal lattice. Diffraction occurs when there are interferences of scattered waves from electrons in all atoms of the parallel planes. These constructive interferences only occur in a few directions, which depend on the atom spacing and the wavelength of the radiation λ. So from an x-ray beam diffracted by a crystalline sample we can measure the distance between adjacent planes constituting its lattice thanks to the Bragg´s equation $2d\sin\theta=n\lambda$. X-ray diffractions methods are based on the analysis of these interference patterns to extract information on atom positions and spacing in a crystalline structure[20].

It is generally hard to obtain single crystals so powder diffraction is more applied for sample analysis. However, in contrast with single-crystal, a powder contains many very small crystals, randomly oriented[21]. Thus, each one gives rise to a characteristic set of peaks in a powder pattern when exposed to the X-ray beam. These peaks can be compared to a database of known diffraction patterns (such as ICDS) or compared against patterns calculated from single-crystal diffraction data in order to identify crystal components present in a bulk powder [20]. Therefore, powder diffraction is a useful tool for gathering information concerning the crystalline composition of a sample. However, it is difficult to solve a complicated structure just by using powder pattern[21]. X-ray diffraction of the powders was performed with the Bruker AXS D8 diffractometer (department of Materials Technology, NTNU) using Cu Kα radiation ($\lambda = 1.54 \times 10^{-10}$ m). The 2θ angle measurements were taken from 10 to 80° and with a path of 0.05°/step.

3.2.2 X-ray fluorescence spectroscopy (XRF)

When a sample is irradiated with x-ray beam, electrons from inner core levels are first liberated, then the vacancies created are filled by electronic transitions from outer levels, resulting in emission of a radiation of lower energy than the primary incident X-ray (fluorescent radiation) by the atoms of the sample. Energy of the emitted photons and the intensity are respectively characteristic and proportional to the concentration of a particular

element. Therefore, XRF spectroscopy is a useful technique to determine the composition and abundance of elements in a sample[22].Approximatively 0.18g of sample was mixed with 2.8g of H_3BO_3 (binder) and turned into a pellet. The analysis was done using the Rigaku SuperMini200 spectrometer.

3.2.3 N_2 adsorption/desorption: BET model

The inert gas N_2 is used as a probe in order to determine the specific surface area of a material. The analysis is performed by recording an isotherm of adsorption of this gas on the solid surface at the temperature of liquid azote (77K). The sorption isotherm is obtained by plotting the amount of adsorbed N_2 as a function of its equilibrium pressure. Different types of adsorption-desorption isotherms are classified according to the IUPAC recommendations and give indication on the material porosity. Indeed, the isotherm type I, showing adsorbed gas saturation, is specific of microporous solids (pore size below 2nm). The isotherm type II showing a constant increase of the adsorbed gas (multilayer of gas molecule adsorbed on the surface) is specific of non-porous or macro porous solids (pore size above 20nm). The isotherms type IV display different hysteresis loops (due to capillary condensation), they are specific of mesoporous solids (pore size between 2 to 20nm). Finally, the unusual isotherm types III and V are mainly observed for adsorption of steam on a hydrophobic surface.

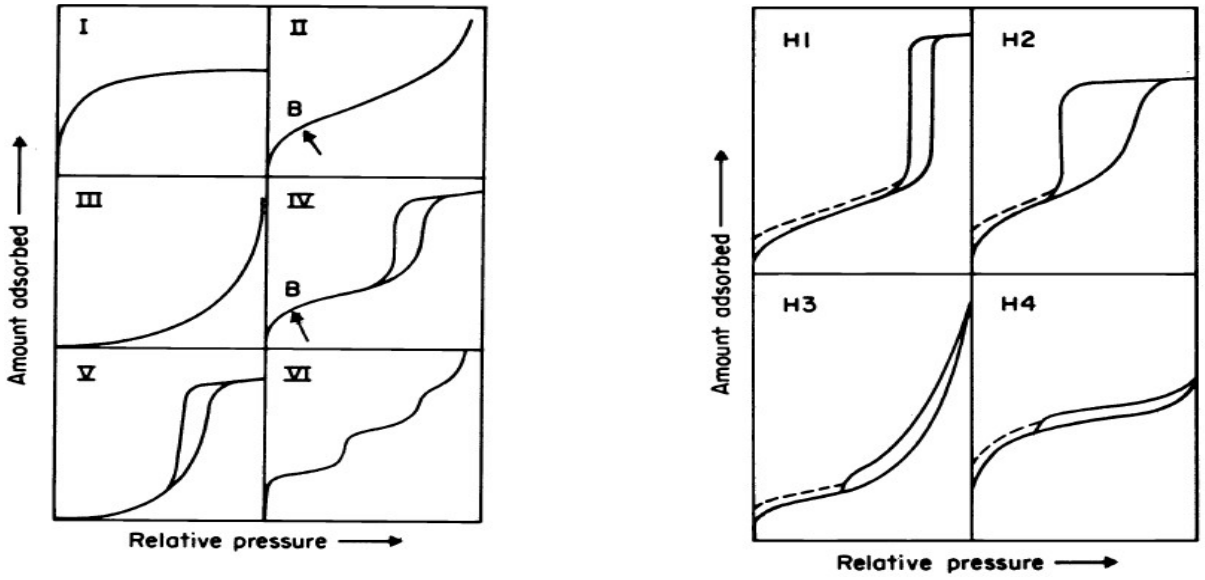

Fig. 3.1: Type of physisorption isotherms and hysteresis loops taken from [23]

Professors Brunauer, Emmett and Teller developed the BET model (1938) in order to extract data especially the surface area (S_{BET}) from type II isotherms[24]. It can also be suitable for type IV isotherms if they display the progressive increase of adsorbed gas (see point B). The model

assumes for the first gas layer adsorbed on the solid surface that there is only one type of adsorption site, there are no interaction between the adsorbed molecules and E_1 is the adsorption energy for the first layer. Then, it assumes that the last adsorbed layer n is liquid so defines E_n (energy of the last adsorbed layer) equals to E_l (energy of liquefaction). The BET equation is defined from these assumptions and by linearization gives the equation 3.1. This last equation, easy to plot, convert the experimental adsorption isotherm into the BET linear equation, making possible to determine the volume of gas requires to form an adsorbed layer, then to get the specific surface area S_{BET} in addition with the pore diameter and pore volume. The Micromeritics TriStar 3020 Surface area and porosity analyser instrument was used to perform sample analysis and the VacPrep 061 Degasser unit for sample pre-treatment under vacuum overnight at 200°C.

$$\frac{P}{V_a\,(P^0-P)} = \frac{1}{C\,V_0} + \frac{(C-1)P}{C\,V_0 P^0} \qquad [3.1]$$

P: Pressure of the probe gas

V_a : Volume of the adsorbed gas

V_0: Volume of adsorbed gas in one monolayer

C: Constant

3.2.4 Scanning electron microscopy – X-ray energy dispersive spectroscopy (SEM-XEDS)

The scanning electron microscope (SEM) uses a focused beam of high-energy electrons at the surface of a solid sample to generate a variety of signals resulting from the interactions between these electrons and the sample atoms[25]. When the electron beam interacts with the surface of the specimen it can be scattered in different directions leading to a range of secondary signals detected to get information concerning the material. For instance, the external morphology (high-resolution image) is observed from detection of secondary electrons, X-rays and visible light. Then, the microstructure and chemical composition is obtained from detection of backscattered electrons by X-ray energy-dispersive spectrometry (XEDS)[26]. The powder was analysed with the Scanning electron microscope SEM Hitachi S-3400N (Department of Material Technology, NTNU).

3.2.5 Ultraviolet-visible absorption spectroscopy : diffuse reflectance spectroscopy

When performing UV-Vis spectroscopy on powder sample, diffuse reflectance, which occurs when the incident light is reflected by the randomly crystals constituting the sample cannot be neglected. In order to correlate reflective to absorption spectra which are obtained by transmittance measurements, the Kubelka-Munk function is applied, see equation[34] [3.2] where $F(R)$ is the Kubelka-Munk function, R is the diffuse reflectance, k is the absorption coefficient, and s is the scattering coefficient. The theory behind this function can be found in reference 33 and 35. A large values of $F(R)$ shows a strong absorption of the incident light by the powder.

$$F(R) = \frac{1-R^2}{2R} \approx \frac{k}{s} \qquad [3.2]$$

The prepared mixed oxide catalysts display colours from light to dark green when increasing the cobalt content (Appendix B). Therefore, they are subjected to diffuse reflectance in the visible wavelength region. Thus, this technique is applied in order to follow the evolution of nickel and cobalt states during the reduction and combustion steps. Moreover, the literature shows application of the reflectance spectroscopy in heterogeneous catalysis, in order to investigate surface species and reactions[35, 36].

The reflectance spectra of the samples were collected by using the AvaSpec-3648 spectrometer by AVANTES. The UV-Vis light probe was directed toward the top of the catalytic bed inside the furnace. The reactor and the furnace apertures were respectively covered with aluminium foil and quartz wool in order to keep the sample under a dark environment. However, the infrared light due to the high temperature inside the furnace (from approximatively 700°C) could not be avoided and is therefore visible in the collected spectra.

3.2.6 Gas chromatography (GC)

A gas chromatograph consists of an injection port, a column and one or more detectors. A fraction of the product stream is injected into a column, which is situated in an oven. After the injection a program governs the temperature in the column, separating the compounds according to their volatility at specific temperatures. A carrier gas, usually inert such as He, Ar or N_2, transports the compounds through the column and past the detector. The column contains a stationary phase, either solid or liquid which delays the passage of the components. The most volatile compounds leave the column first. The GC used during this master thesis

possesses two detectors: the thermal conductivity detector (TCD) and the flame ionization detector (FID) which is sensitive to most organic components. The GC analysis provides a chromatograph with peaks. A peak identifies the species and the area of the peak indicates the relative amount of this species[27]. Therefore, gas chromatography is a useful technique for the identification and quantitative analysis of gas phase products during a reaction. However, it does not identify compounds, which have not been added during the calibration of the instrument.

3.3 Activity of the catalysts

Methane combustion was carried out in a fixed-bed quartz reactor. The Ni-Co mixed oxide catalyst was diluted 20 times in α-Al_2O_3 (0,15g catalyst for 3g alumina) and the pellet size range from 75 to 150 μm. The catalyst was reduced under a gas flow composed of 75ml/min H_2 and 75ml/min Ar at 670°C for 16h using a heating rate of 2°C/min. Then the reduced catalyst was kept under 75ml/min Ar for 2h before starting the reaction. The reactant mixture ratio CH_4:O_2 was fixed to 1:2.5. Thus, the total gas flow mixture fixed to 300 mL/min was composed of methane (10,5ml/min), air (125ml/min) and argon (164,5ml/min) as inert. Prior starting the experiments, a leak test of combustible gas was performed for the whole system with a toxic gas detector OLDHAM TOXIMETRE TX2000. The gas flow is controlled with mass flow controllers (MFC) calibrated with a bubble flow meter. The calibration curves are included in the Appendix D.

The methane oxidation was followed by gas chromatography. The instrument Agilent 6890N Gas Chromatograph was calibrated with the reactants and the products of the reaction namely CH_4, O_2, Ar, H_2, CO and CO_2. Finally, the methane conversion and selectivity towards CO were calculated based on the integrated GC (TCD) peak areas, which provide the volume percentages (C_i) of the detected compounds.

$$C_i = A_i \times RF_i$$

Where A_i is the integrated area of a compound *i* and RF_i is the respond factor of a compound *i.*

The conversion of methane is calculated as follow:

$$X_{CH4} = \frac{C_{CO} + C_{CO}}{C_{CH4} + C_{CO2} + C_{CO}} \times 100$$

The selectivity towards CO is calculated as follow:

$$S_{CO} = \frac{c_{CO}}{c_{CO}+c_{CO_2}} \times 100$$

The temperature profiles of the catalytic beds were reported by moving the thermocouple at each 0,5cm path and at different furnace temperature. No temperature profiles for the 5 and 12wt% metal loading catalysts were reported because of experimental problems when analysing the catalytic bed by UV-Vis spectroscopy.

4. RESULTS AND DISCUSSION

4.1 XRD patterns

The XRD patterns of the prepared 5wt% Ni-Co hydrotalcite like compound (HTlcs) are presented in Fig 4.1. These non-calcined samples show general features that are typical of all HTlcs[11, 28], which are the presence of specific sharp and intense peaks at low 2θ. For example, the sharp peaks at 2θ equal 11°, 22° and 35° respectively correspond to the (003), (006) and (009) crystal planes, which indicate relatively well defined layered structures. Moreover, the broad and asymmetric peaks at 2θ equal 38° and 46° correspond to (015) and (018) crystal planes[11]. The diffraction patterns also reveal that the degree of crystallization of the HT structure depends on the Co and Ni contents. Indeed, the bimetallic hydrotalcites, which show sharp and high peaks, indicate a better crystallinity of their hydrotalcite structure. The ion radius of the cations can explain this observation. Indeed, Ni^{2+} has a radius of 0.72 closer to Mg^{2+} (0.65) and Al^{3+} (0,60) compared to Co^{2+} ion radius of 0,74. Therefore, it is relatively easy to incorporate Ni^{2+} in the hydrotalcite lattice compared to Co^{2+} ions, which distort the HT structure when inserted in the layers, resulting in a low crystallinity. This feature is well observed in the XRD patterns of the 12wt% loading catalysts Fig 4.4 and in a less extent in Fig 4.5 for the high metal loading catalysts. Indeed, samples containing more nickel than cobalt display higher and sharper peaks. This result is not obvious for the 5wt% loading catalysts; it shows that Co does not distort the structure when present in low loading.

After thermic treatment of the samples at 600°C, the diffraction patterns in Fig 4.2 do not show peaks of the hydrotalcite structure.. Besides the patterns displays severe overlapping of peaks corresponding to different magnesium, aluminium, nickel and cobalt oxides. These results confirmed the transformation of hydrotalcite compounds into mixed metal oxides in addition with a decrease in the material crystallinity. In the diffraction pattern of the 5wt% Ni

mixed oxide, NiO, $MgNiO_2$ and MgO compounds may be present as they are identified in the overlapped large peaks. In samples containing cobalt, peaks of CoO and Co_2O_3 are hardly identified in the diffraction patterns. However, these peaks can be attributed to spinel phases Co_3O_4, $MgCo_2O_4$, $CoAl_2O_4$, Co_2AlO_4 and/or $NiCo_2O_4$ but it is not possible to distinguish them, as they are overlapped. Both He[28] and Lim[8] emphasize these observations, which confirm the formation and stabilization of spinel phases derived from HTlcs. Moreover, increasing the Ni-Co loading is displayed in the pattern by sharper but still overlapped peaks, Fig 4.3. However, XRD pattern of the 20, 30 and 40 wt% Ni-Co mixed oxides which were used during thesis in Fig 4.4 shows that increasing the metal loading and Co content better display peaks of spinel phases.

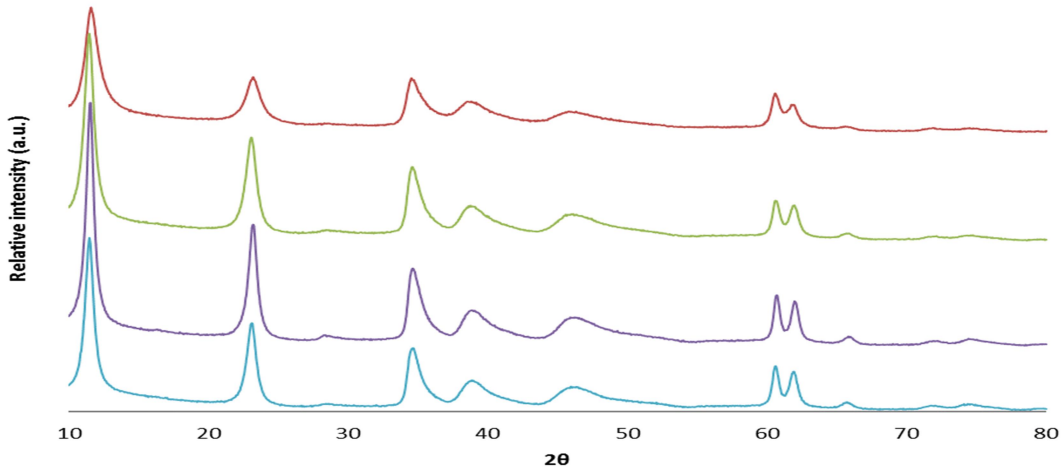

Fig. 4.1: XRD patterns of (a) 3.5Ni-1.5Co, (b) 2.5Ni-2.5Co, (c) 1.5Ni-3.5Co and (d) 5Co hydrotalcite precursors.

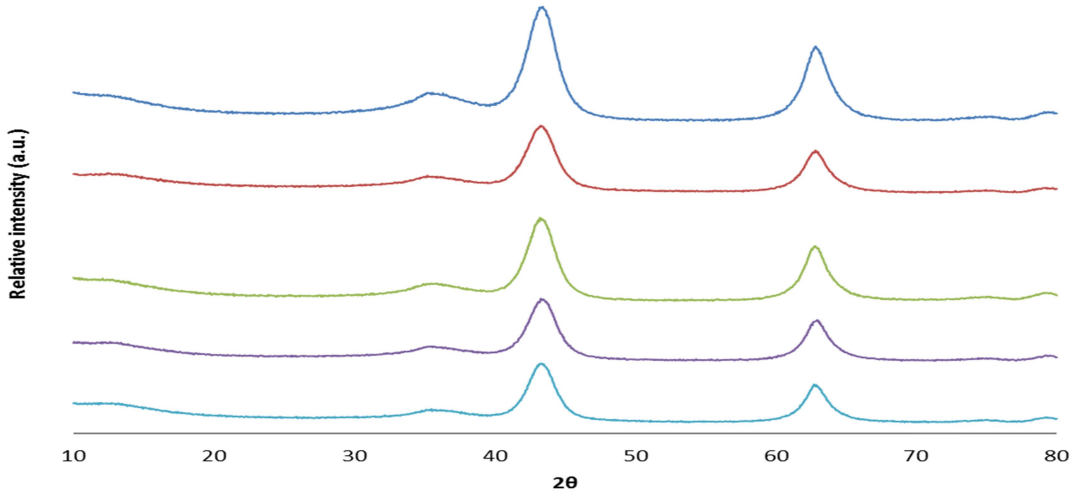

Fig. 4.2: XRD patterns of (a) 5Ni, (b) 3.5Ni-1.5Co, (c) 2.5Ni-2.5Co, (d) 1.5Ni-3.5Co, and (e) 5Co mixed oxides obtained after calcination of their respective hydrotalcite precursors.

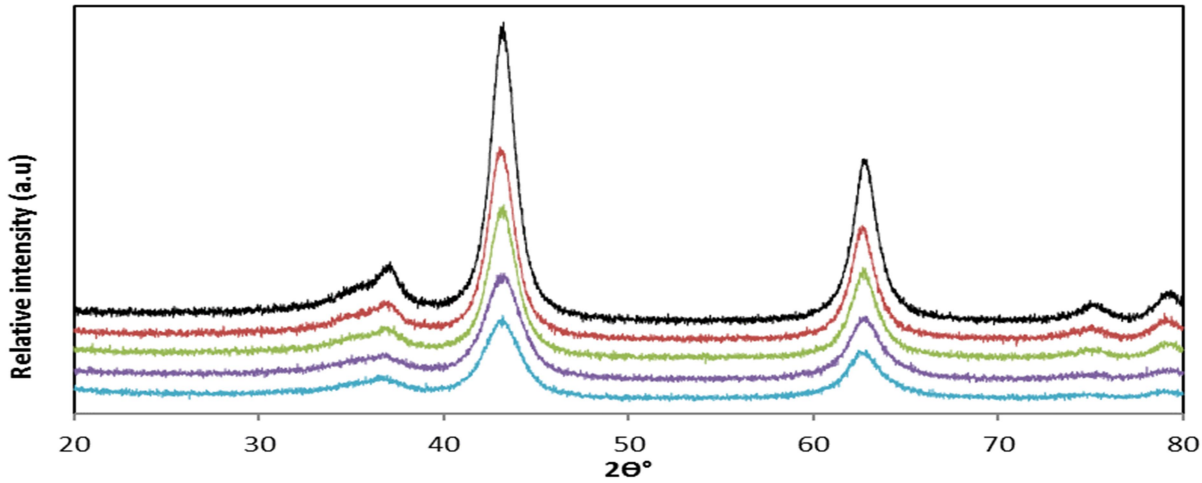

Fig. 4.3: XRD pattern of the 12wt% loading catalysts investigated in this thesis. From the top to the bottom, 12Ni, 9Ni-3Co, 6Ni-6Co, 3Ni-9Co and 12Co mixed oxides (samples of PhD student Shirley E. Liland).

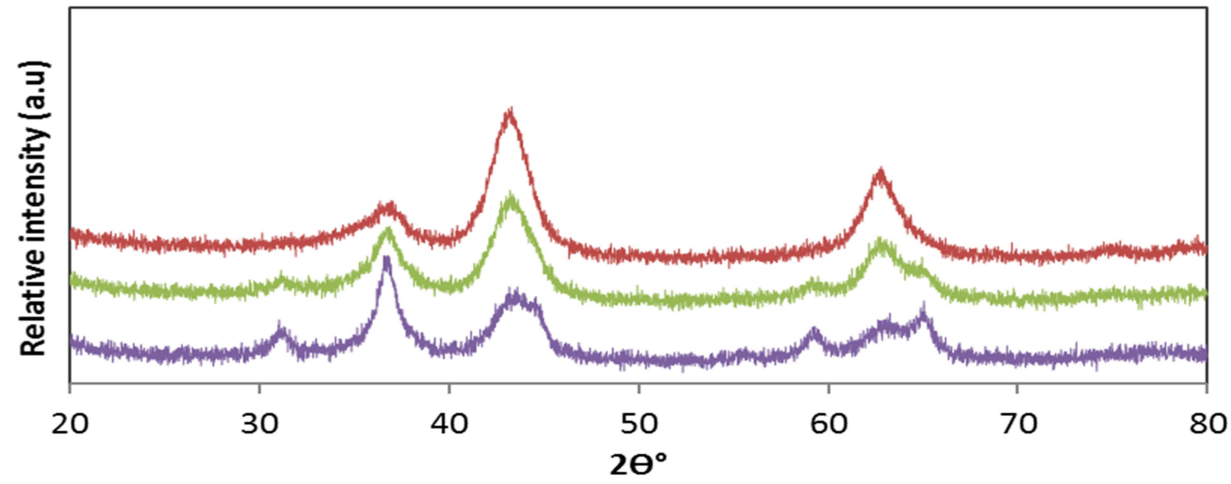

Fig. 4.4: XRD pattern of the 20, 30 and 40wt% Ni-Co catalysts investigated in this thesis. From the top to the bottom: 6Ni-14Co, 9Ni-21Co, 12Ni-28Co mixed oxides (from former master student Bilal Yousaf)[48].

4.2 XRF data

Chemical composition of the prepared 5wt% Ni-Co catalysts was determined by XRF. The data show incorporation of Ni and Co in all the samples. Moreover, sodium is not detected, which confirms the elimination of this element during the filtration step. Indeed, sodium is a poison for this type of catalysts derived from thermal decomposition of hydrotalcite precursors[11]. However, the quantitative analysis of the samples in Table 4.1 does not agree with the theoretical composition of the prepared materials because it displays lower Ni and Co contents. Table 4.2 shows the XRF analysis of the aqueous solution after filtration of the reactant mixtures for the respective preparation of 1.5Ni-3.5Co and 2.5Ni-2.5Co hydrotalcite

precursors. The data show the presence of sodium in these solutions. Therefore, it shows that this element is not incorporated in the materials. Moreover, we observe that small amount of magnesium is lost during the preparation. Finally, Ni and Co are not detected which suggests they can be totally incorporate in the prepared materials (or due to the large range error of the apparatus), therefore the low Ni and Co amount displaying by the XRF analysis of the sample pellets may not due to the loss of these metals during synthesis. In short, in this thesis the purpose of powder XRF analysis was about qualitative information rather than quantitative one.

Table 4.1: Composition of the 1.5Ni-3.5Co and 2.5Ni-3.5Co hydrotalcite precursors.

	Results (mass %)		**El.line**
Component	**1.5Ni-3.5Co powder pellet**	**2.5Ni-2.5Co powder pellet**	
MgO	68,13	68,91	Na-Kα
Al_2O_3	28,37	27,31	Mg-Kα
SiO_2	0,66	0,45	Si-Kα
K_2O	0,29	0,38	K-Kα
Co_2O_3	1,83	1,49	Co-Kα
NiO	0,72	1,45	Ni-Kα

Table 4.2: Composition of the aqueous solution after filtration of the hydrotalcite precursors 1,5Ni-3,5Co and 2.5Ni-3.5Co.

	Results (mass %)		**El.line**
Component	**1.5Ni-3.5Co aqueous solution**	**2.5Ni-2.5Co aqueous solution**	
Na	14.76	14.28	Na-KA
Mg	0.43	0.47	Mg-KA
Si	0.04	0	Si-KA
K	0.06	0.06	K-KA
H_2O	84.71	85.19	

4.3 SEM-XEDS data

The SEM picture and XEDS analysis of the mixed oxides 1.5Ni-3.5Co and 3.5Ni-1.5Co are shown in Fig 4.5, 4.6 and tables 4.3 and 4.4. The compositions of the samples given by the EDS confirm the presence of the elements constituting the desired mixed oxides catalysts namely carbon, oxygen, magnesium, aluminium, cobalt and nickel. However, it is remarked

that the nickel and cobalt content is slightly higher than the five-weighted percentage expected as it represents approximatively 6wt%. However, the proportion between nickel and cobalt is respected. Indeed, the analysis for 1.5Ni-3.5Co shows that nickel and cobalt respectively represents 30 and 70% of the total metal loading; and inversely for the 3.5Co-1.5Co. The liquid XRF analysis of the filtrated mixture showed that a small quantity of magnesium is not incorporated in the hydrotalcite structure; this observation can explain the increase of the nickel cobalt content displays by the XEDS analysis.

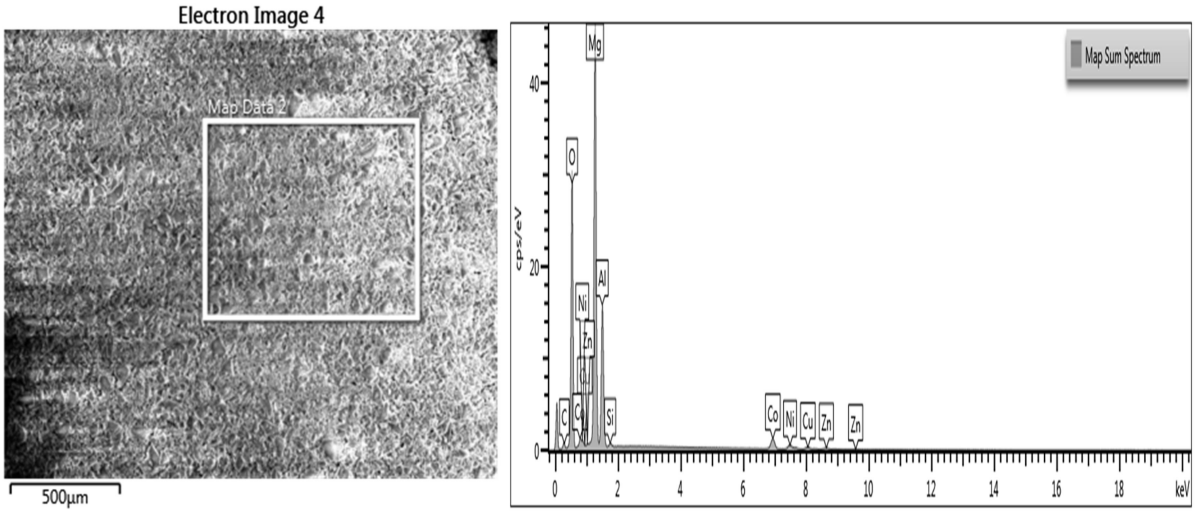

Fig 4.5: SEM picture and XEDS spectra of 1.5Ni-3.5Co hydrotalcite precursor.

Table 4.3: Composition of the 1.5Ni-3.5Co hydrotalcite precursor given by XEDS.

Elements	C	O	Mg	Al	Si	Co	Ni	Cu	Zn	Total
Weight percent (%)	5.65	40.13	31.26	14.32	0.33	4.1	1.87	1.27	1.07	100

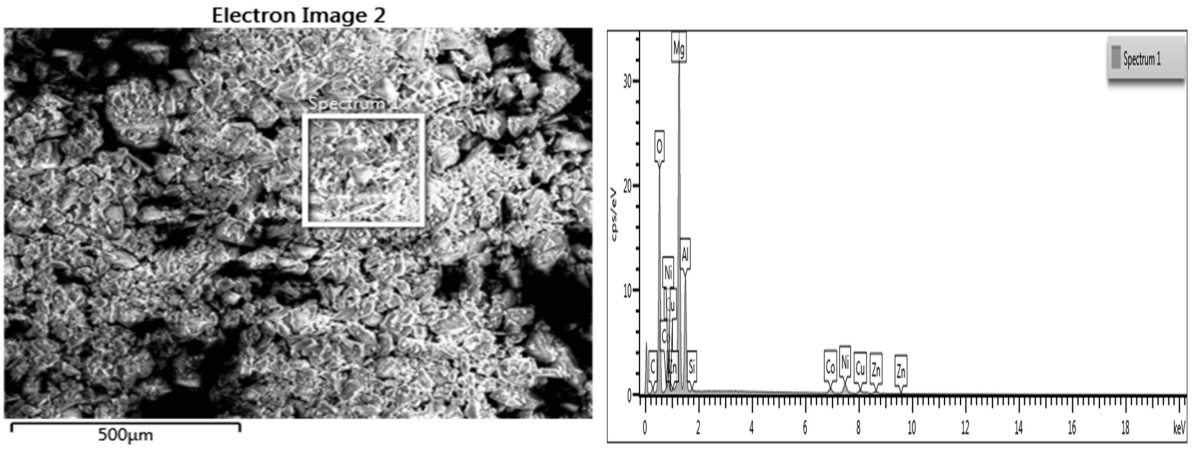

Fig. 4.6: SEM picture and XEDS spectra of the prepared 3.5Ni-1.5Co hydrotalcite precursors.

Table 4.4: Composition of the 3.5Ni-1.5Co hydrotalcite precursor given by XEDS.

Elements	C	O	Mg	Al	Si	Co	Ni	Cu	Zn	Total
Weight percent (%)	5.67	38.25	31.57	13.74	0.22	2.1	4.66	2.25	2.01	100

Finally, XEDS data show unexpected high amounts of copper and zinc in the samples. These elements are assumed impurities of the powder reactants. Indeed, the supplier MERCK indicates Zn and Cu among impurities present in NaOH pellets.

4.4 N_2 adsorption/desorption

The N_2 adsorption –desorption isotherms of the prepared mixed oxides are shown in Fig 4.7. According to the IUPAC classification, their shape can be assigned to type IV isotherms with type H3 hysteresis loop. These observations are characteristic of mesoporous materials having a heterogeneous distribution of pore size. Moreover, the observed closing of hysteresis loop at P/P° from 0.55 to 0.6 is a feature of oxides derived from hydrotalcites, which is due to the presence of pores open at both ends[12].

The BET surface areas (S_{BET}), average pore diameter (D_p) and pore volumes (V_p) of the tested mixed oxide catalysts are listed in table 1. The S_{BET} ranges from 191.2 to 235.3m^2/g. For comparison the N_2 adsorption experiment of the hydrotalcite precursor 2.5Ni-2.5Co was performed, Fig 4.8. It displays a S_{BET} of 112m^2/g which is increased until 233 m^2/g when transformed to mixed oxide after the thermic treatment at 600°C for 16h.This evolution is in agreement with the properties of mixed oxides derived from hydrotalcites described by Cavani[11]. Furthermore, Bellotto and al demonstrated that the increase of surface area is mainly due to the breakdown of the initial hydrotalcite layer structure when transformed to mixed oxide at high temperature. It is also observed that the surface area decreases with the increasing the nickel cobalt loading, it indicates that these elements influence the textural properties of the mixed oxides as they form crystalline phases, thus lower the surface area of the material. Moreover, He and al[28] explained that the cobalt promotes spinel phases and the XRD patterns of the mixed oxide catalysts also reveal that nickel spinel phases can be present in their structure. Finally, the pore diameters of these mixed oxides range from 8.2 to 12 nm, which confirm the mesoporous nature of these materials.

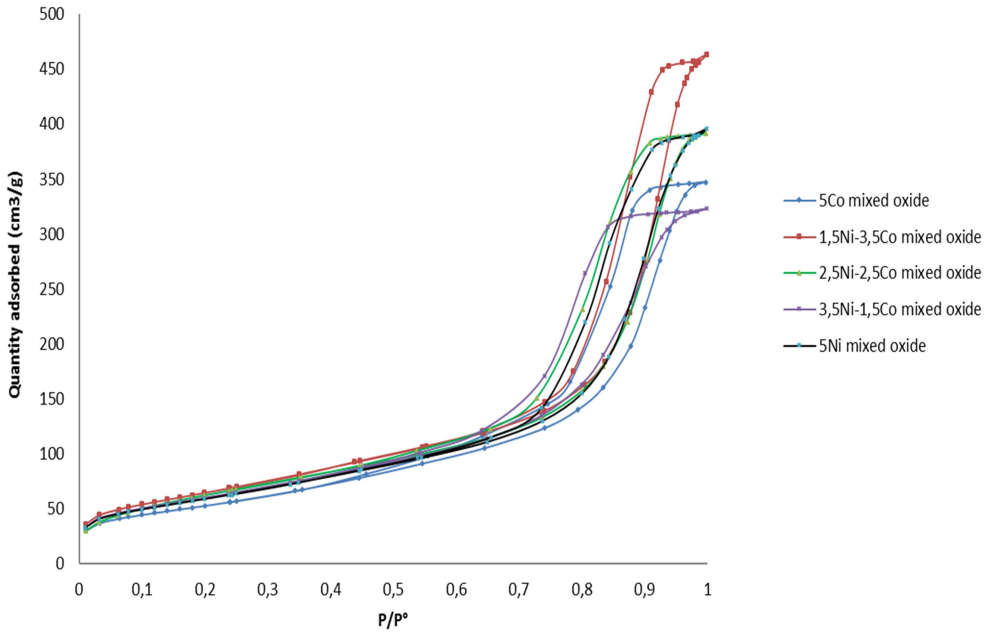

Fig. 4.7: N_2 adsorption Isotherms of the prepared mixed oxide samples.

Table 4.5: Structural parameters: specific surface area (S_{BET}), pore diameter (Dp) and pore volume (Vp) of the prepared 5wt%Ni-Co mixed oxide catalysts.

Mixed oxide samples		N_2 adsorption- desorption		
		S_{BET} (m^2/g)	D_p (nm)	V_p (cm3/g)
5wt%	5Ni	213.5	11.3	0.60
	3.5Ni-1.5Co	217.3	9.2	0.5
	2.5Ni-2.5Co	233.6	10.4	0.61
	1.5Ni-3.5Co	235.3	12	0.70
	5Co	191.2	8.2	0.54

Table 4.6: Structural parameters of the 12, 20, 30 and 40wt% Ni-Co mixed oxide catalysts tested for methane combustion.

Mixed oxide samples		S_{BET} (m^2/g)
12wt%	12Ni	138
	9Ni-3Co	146
	6Ni-6Co	155
	3Ni-9Co	171
	12Co	170
20wt%	6Ni-14Co	166,00
30wt%	9Ni-21Co	138,00
40wt%	12Ni-28Co	114,00

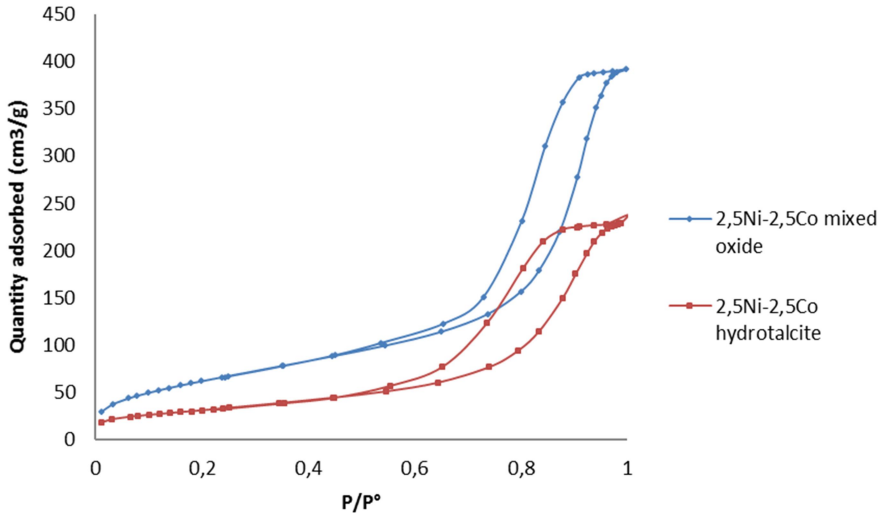

Fig. 4.8: N_2 adsorption-desorption isotherm of the 2.5Ni-2.5Co hydrotalcite based catalyst before and after treatment at 600°C for 6h.

4.5 Activity and evolution of the catalysts

4.5.1 Activity and evolution of the catalysts

The UV-Vis spectra of the 5Co and 5Ni catalysts are shown in Fig 4.9 and Fig 4.10. It is observed that during the reduction of the catalysts the intensity of the reflectance curves decreases until a stabilized value of approximatively 20% for 5Co and 5% for 5Ni samples. During methane combustion the opposite occurs, indeed the intensity of the reflectance curves increases with the furnace temperature. The high reflectance intensities near infrared region are due to the furnace infrared light at high temperature, which could not be prevented. These observations showed that reduced nickel and cobalt less reflect the light compared to their oxidized states. Therefore, the evolution of the catalysts during the reduction and the methane combustion was followed with the UV-Vis light spectroscopy. Thus, two tendencies are observed during the reduction of 5Co mixed oxide catalysts. Firstly, there is an increase of reflectance from room temperature to approximatively 500°C. On the other hand, the reflectance decreases from 500°C to 670°C. The XRD of the samples and the literature[5, 8,11,28] show that the cobalt catalysts derived from hydrotalcite precursors are composed of some spinel cobalt oxides, therefore they contain both Co^{2+} and Co^{3+} ions. Consequently, this

evolution in the reflectance spectra can be attributed to the passage from Co^{3+} to Co^{2+} at the beginning of the reduction step, following by the Co^{2+} to Co^{0} transition. This spectral feature during the reduction step is also observed in the bimetallic samples containing high cobalt content such as 3Ni-9Co and 1,5Ni-3,5Co, which confirms that cobalt is firstly reduced following by nickel. The 5Ni catalyst does not display this oscillation in the reflectance; therefore, it confirms that only transitions between Ni^{2+} and Ni^{0} state occur.

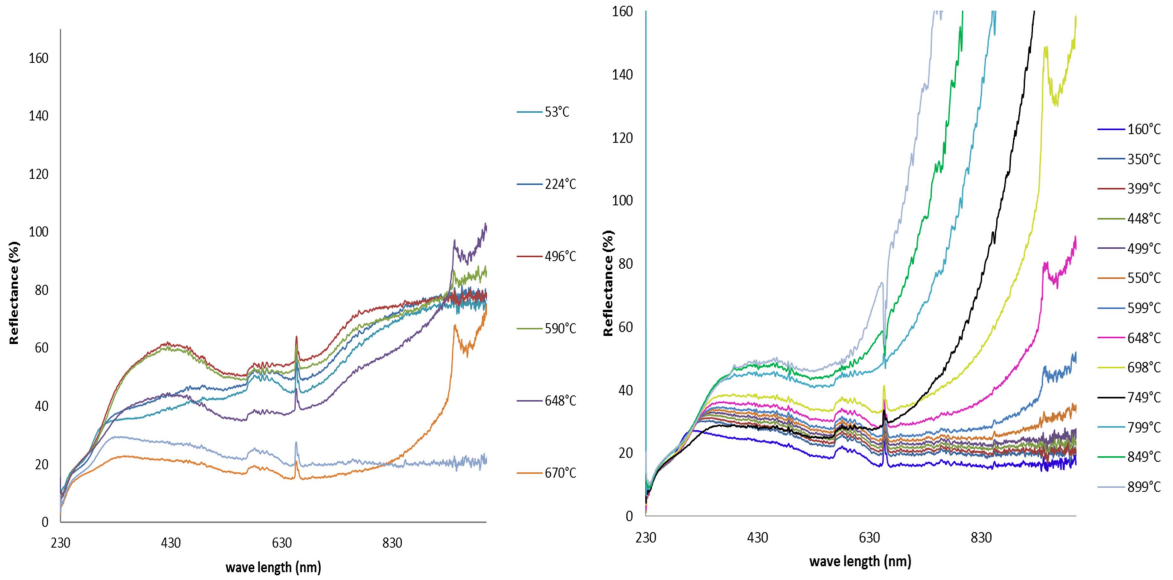

Fig. 4.9: UV-Vis spectra of the 5Co mixed oxide catalyst during reduction step (left) and methane combustion (right) at different furnace temperatures.

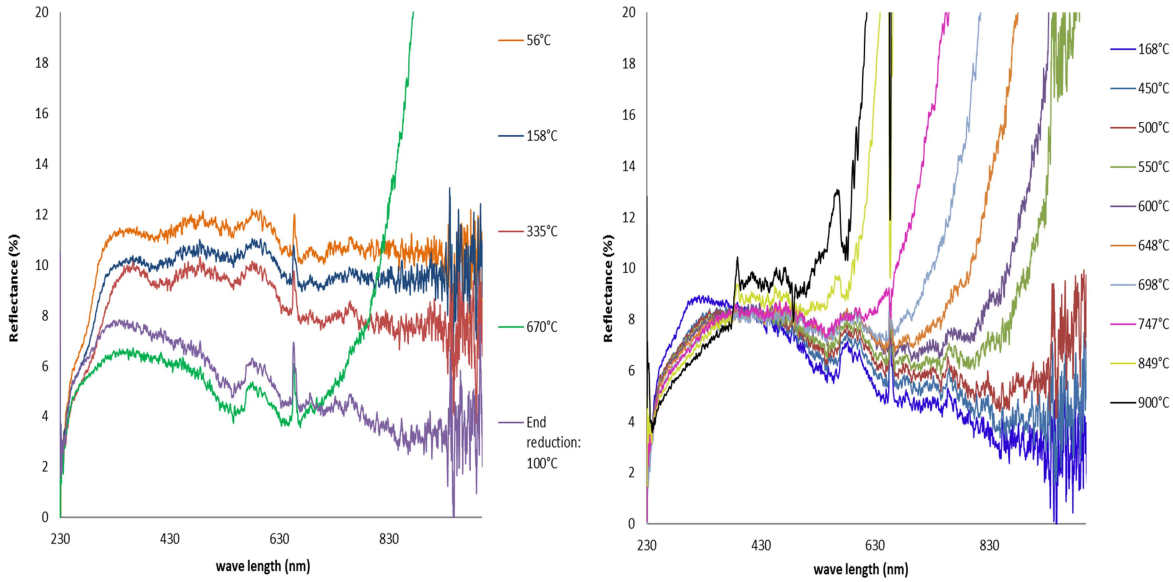

Fig. 4.10: UV-Vis spectra of the 5Ni mixed oxide catalyst during reduction step (left) and methane combustion (right) at different furnace temperatures.

The temperature profiles of the catalytic beds of the 20, 30 and 40wt% Ni-Co mixed oxide catalysts with Ni/Co proportion 30:70 at 700°C is shown Fig 4.11. The variation of temperature between the furnace and the catalytic bed is maximal from 1.4 to 1.9 cm in the catalytic bed, knowing that its height is 2.7cm. These temperature profiles show that methane combustion mainly occurs in the middle of the catalytic bed for high Ni-Co loading catalysts. Therefore, it shows the presence of hot spots in the bed. The temperature profile of the 40wt% bimetallic at different furnace temperature Fig 4.12 shows that hot spots start occurring around 600°C which correspond to 53% methane conversion.

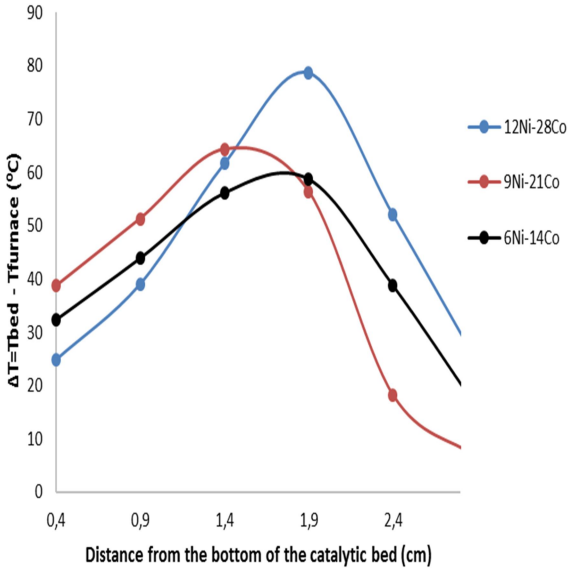

Fig 4.11: Temperature profiles of the 12Ni-28Co, 9Ni-21Co and 6Ni-14Co diluted in α-Al203 catalytic beds at 700□C.

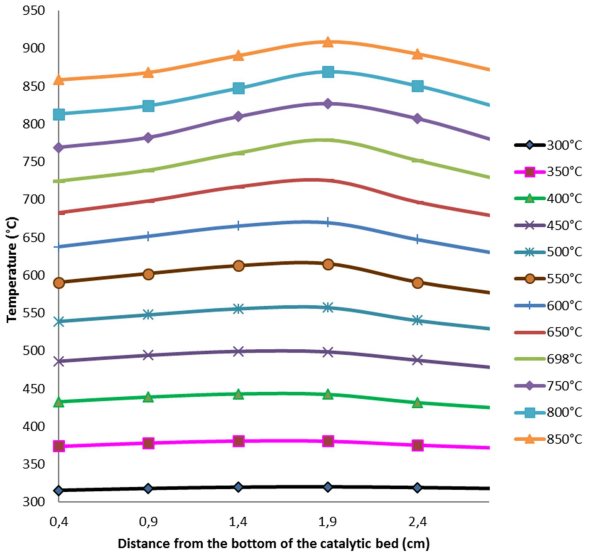

Fig. 4.12: Temperature profile of the catalytic bed 6Ni-14Co mixed oxide catalyst at different furnace temperatures.

Methane conversion as a function of the furnace temperature for the tested 5wt% loading catalysts are shown in Fig 4.13. The 5Ni mixed oxide is not included as the chromatograms displays unknown peaks (Appendix D) which did not permit to calculate the methane conversion with accuracy. These noise peaks also appeared in chromatograms of other tested catalysts but usually disappeared at high temperature. The bimetallic 2.5Ni-2.5Co displays better activity on methane oxidation. Moreover, the Fig 4.14 which shows the calculated oxidized surface of the 5wt% loading catalysts versus the combustion temperature based on the UV-Vis spectroscopy (see Appendix F) confirms that the methane conversion is related to the oxidation of the active phase. Indeed, we observe that the conversion is low when the active phase is less oxidized or remains in the metallic state (negative fraction of oxidized surface). Furthermore, the shapes of the oxidized surface curves surprisingly follow the

methane conversion over these catalysts. Therefore, oxide phases are required in order to achieve high methane conversion. However, a drop in the conversion is remarked around 700 and 750°C for the 5Co, 1.5Ni-3.5Co catalysts, similarly to 12wt% loading catalysts 3Ni-9Co and 9Ni-3Co, Fig 4.15. Higher metal loading catalysts with 30%Ni-70%Co (20, 30 and 40wt%) do not displays this feature, as methane conversions increase linearly with the temperature, Fig 4.16. Moreover, oxidation of their active phases Fig.4.17 increases with the combustion temperature and do not display diminution at high temperature. Same observation for the 12Ni-25% of the surface coated with Pd which displays the best activity on methane combustion, see Fig 4.15. Thus, an assumption made is the role of Pd in intensification the oxidation of Ni. Therefore, the drop in the methane conversion observed for the low metal loading catalysts can be related to the fluctuation in the light reflectance curves and the fraction of oxidized surface. Two assumptions are discussed to explain the phenomenon.

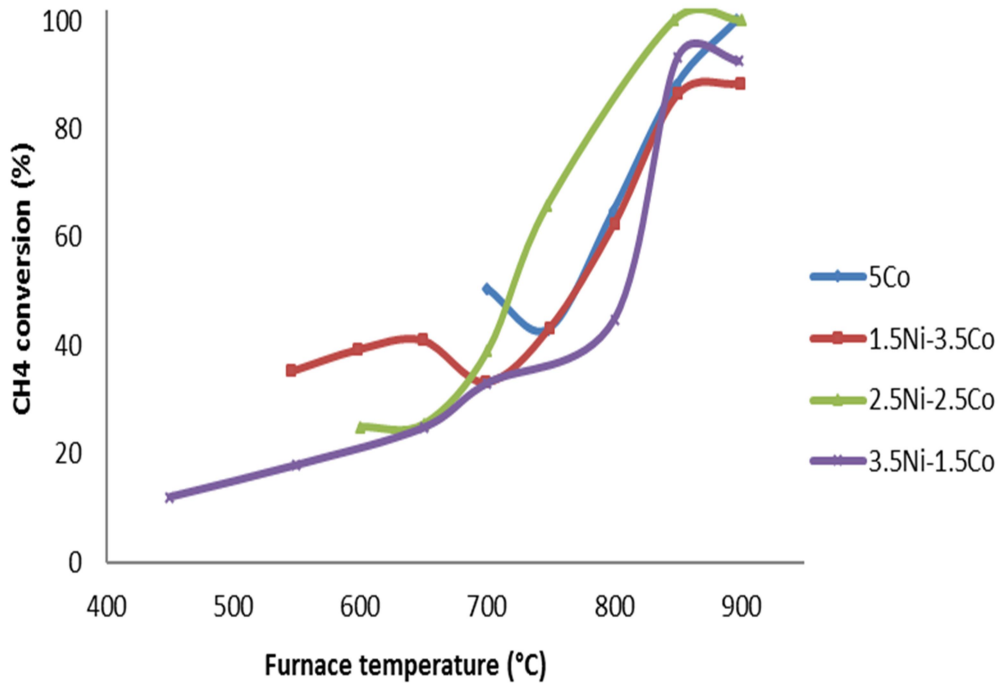

Fig 4.13: Methane conversion as a function of the furnace temperature for the 5wt% Ni-Co mixed oxides catalysts. The 5Ni was not plotted as its chromatograms displays "noises" which did not permit to calculate the conversion of methane with accuracy (See Appendix C).

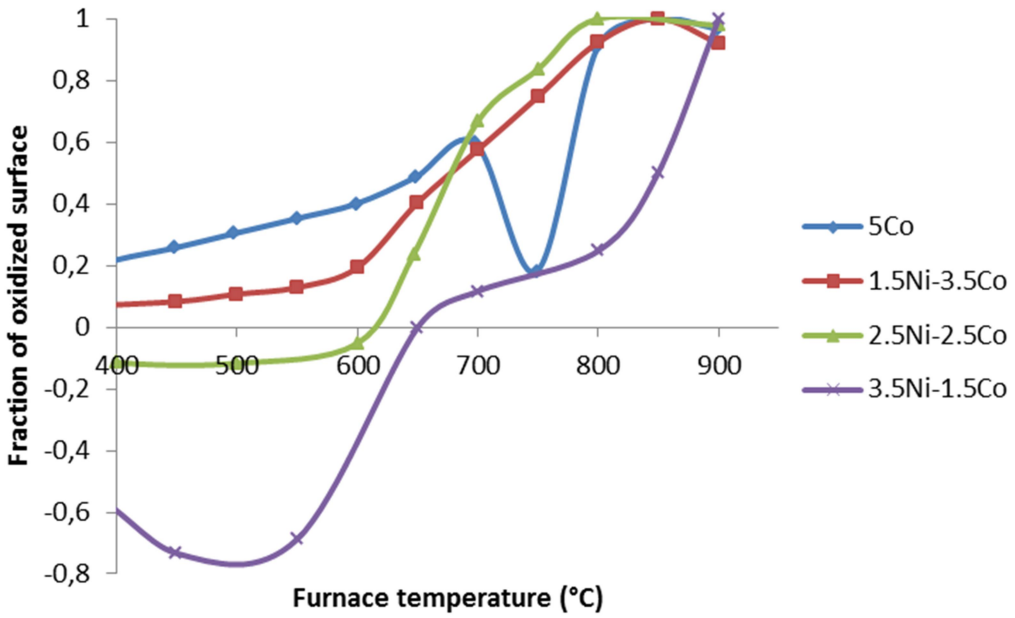

Fig 4.14: Estimation of the fraction of oxidized surface on the 5wt% metal loading catalysts as a function of the furnace temperature during methane combustion experiments. Calculations can be found in Appendix F.

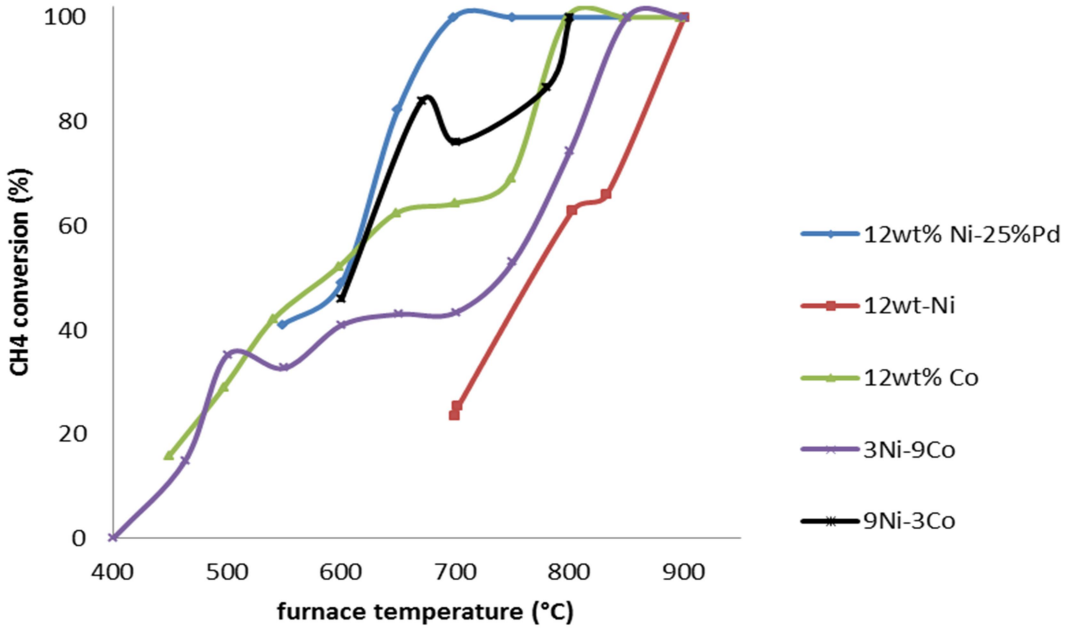

Fig 4.15: Methane conversion as a function of the furnace temperature for 12wt% Ni-Co and Pd mixed oxides catalysts. The bimetallic 6Ni-6Co was not reported as their chromatograms displays "noises" which did not permit to calculate the conversion of methane with accuracy (See Appendix C).

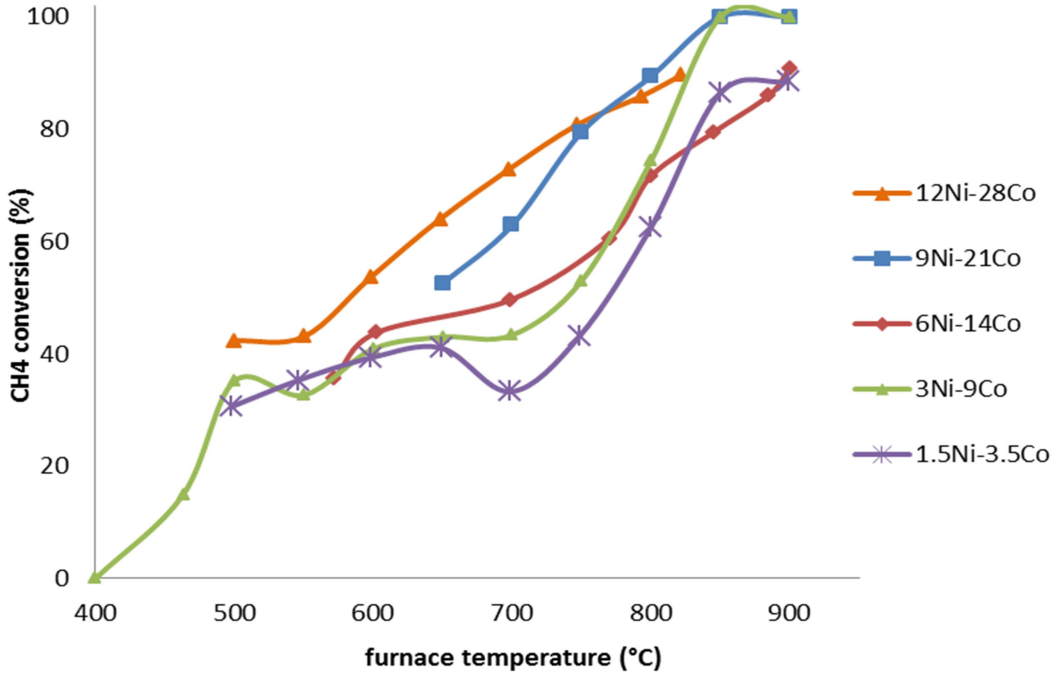

Fig 4.16: Methane conversion as a function of the furnace temperature for 5, 12, 20, 30 and 40wt% Ni-Co mixed oxides with a metal loading proportion of 30%Ni-70%Co.

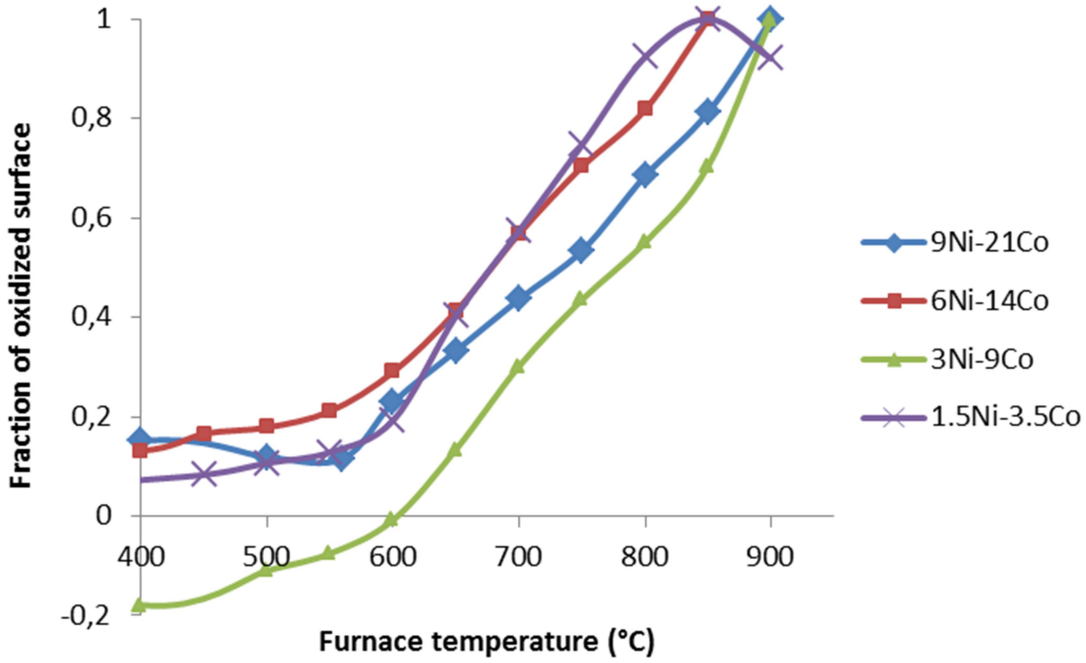

Fig 4.17 Estimation of the fraction of oxidized surface on the 5, 12, 20 and 30 Ni-Co mixed oxides with a metal loading proportion of 30%Ni-70%Co as a function of the furnace temperature during combustion experiments.

4.5.2 Cyclic oxidation/reduction process

It is previously notified a drop in the methane conversion over the 3Ni-9Co, 9Ni-3Co, 5Co and 1.5Ni-3.5 catalysts. These catalysts display high reflectance when increasing the temperature, Fig 4.18 and Fig 4.19. However, their reflectance percentage never increases beyond the maximal value observed during the reduction step. Even for the 9Ni-3Co catalyst, which show a decrease of the reflectance when reducing the combustion temperature from 700°C to 500°C. Furthermore, the decrease in reflectance at 750°C for 5Co catalyst Fig 4.15 can be related to the drop in the methane conversion over this catalyst. This observation shows that partial reduction/oxidation forming especially CoO particles occurs during the methane combustion and this phenomenon depends on the temperature of combustion. It also shows that methane is used as reducing agent rather than reactant for combustion. Moreover, the gas chromatograph showed production of CO above 700°C. These data can explain the oscillation in the methane conversion and the production of CO, which is observed above 700°C.

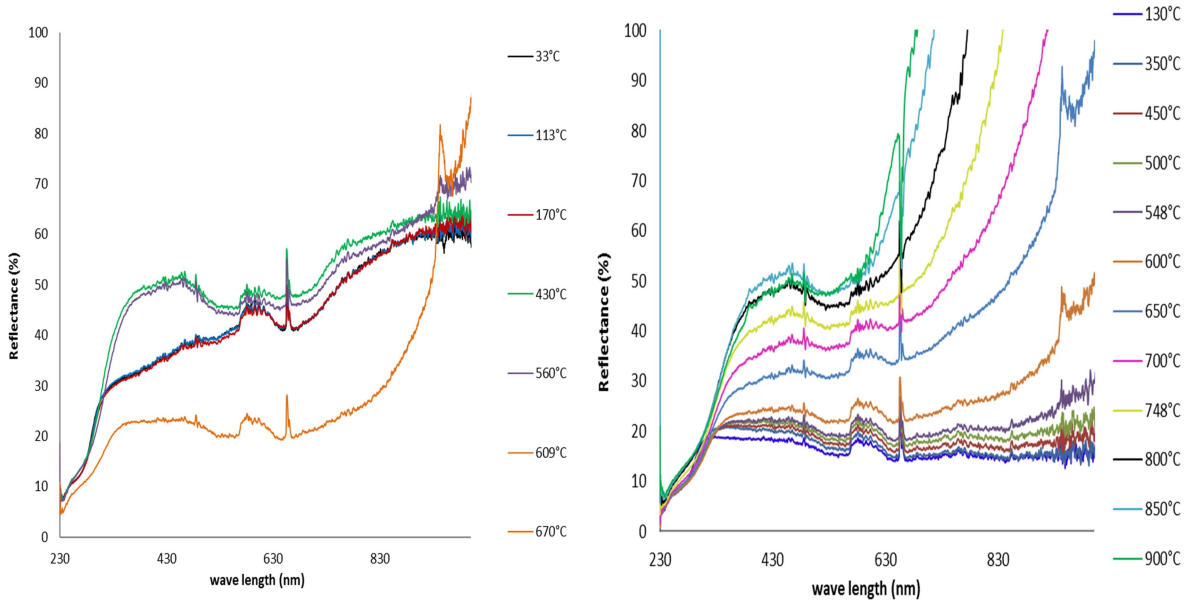

Fig 4.18: UV-Vis spectra of the 1.5Ni-3.5Co mixed oxide catalyst during reduction (left) and methane combustion (right) steps at different furnace temperatures.

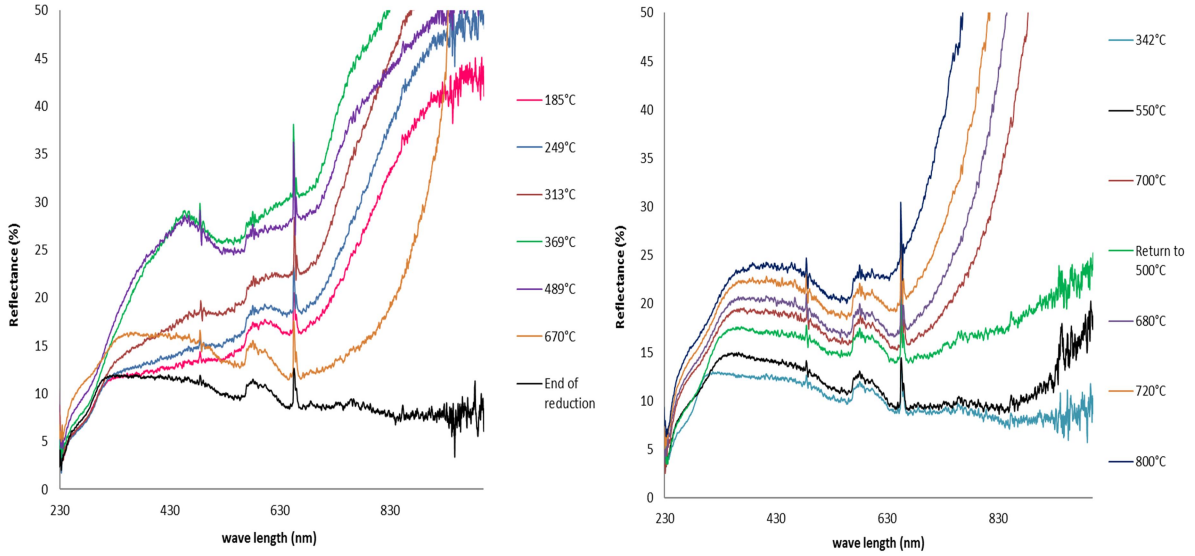

Fig 4.19: UV-Vis spectra of the 9Ni-3Co mixed oxide catalyst during reduction (left) and methane combustion (right) steps at different furnace temperatures.

Thus, a cyclic oxidation/reduction process of the Ni and Co surface can explain these two features observed during the methane combustion. Oscillations in methane oxidation rate over various catalysts such as Pd, Ni and Co have been observed and studied by Zhang and al[37]. They explained that these oscillations arise from repetitive cycles of oxidation and reduction of the catalyst metal surface. Moreover, they mentioned that only a certain part of the surface is responsible for these oscillations whereas others remain permanently in the oxide state. For high metal loading catalysts namely 20, 30 and 40wt% these oscillations are not observed, then their XRD patterns better display peaks of spinel structures. Therefore, it shows that nickel and cobalt are mainly trapped into spinel structures so they are hardly reduced. Thus, they are more stable and less susceptible to undergo a cyclic oxidation/ reduction process. Finally, Zhang and al also remarked that for Ni and Co based catalysts, oxide surfaces produce mainly CO_2 and H_2O, whereas metallic surfaces favour partial oxidation of methane to CO and H_2. For the investigated catalysts during this thesis, production of CO above 700°C is noticed when the reflectance intensity starts being in the CoO assumed reflectance range. Therefore, it is assumed that CO is produced because of the presence of CoO particles or some metallic Ni/Co. Indeed, Khoshandam and al[47] who studied the reduction of CoO with methane defined the chemical equation occurring during this process (Equation 4.1) showing also the formation of CO and Co^0. However, H_2 is not observed in the chromatograms at these combustion temperatures, it can be also use as reducing agent when formed or transformed to H_2O. Table 4.7 shows the selectivity of the catalysts towards CO. It is remarked that bimetallic catalysts with low metal loading and Ni catalysts produce CO. The good activity of

Ni on partial oxidation of methane is known[49]; therefore, it can be assumed that the Ni activity is increased because of the partial deactivation of Co.

$$CoO_{(s)} + CH_{4(g)} \rightarrow Co_{(s)} + CO_{(g)} + 2H_{2(g)} \quad [4.1]$$

Table 4.7: Selectivity towards CO during methane combustion experiments over tested catalysts in which GC detected CO.

	CO selectivity (%)					
Furnace temperature (°C)	12Ni	3.5Ni-1.5Co	2.5Ni-2.5Co	1.5Ni-3.5Co	5Co	5Ni
700	13,2	0	0	0	0	0
750	0	0	7,5	0	0	0
800	18,1	12,2	0	8,7	5,7	0
850	0	0	0	0	7,5	3,7
900	7,3	0	0	0	0	0

4.5.3 Deactivation of the bimetallic catalysts

Another theory investigates to explain the evolution of the reflectance intensity and the drop in the methane conversion is the deactivation of the catalyst. In one hand, it is due to coke formation on the surface of the catalysts. Indeed, it is well-known that this carbonaceous deposit occurring during the transformation of organic compounds at high temperature leads to deactivation of a catalyst[38]. Nevertheless, Alenazey and al[39] who studied the coke removal from Co-Ni based catalysts under O_2, Air, CO_2 and H_2 gas flow mentioned some carbon gasification reactions (equations 4.2 and 4.3) that may occur based on the study of Figueiredo[40]. Thus, carbon gasification can explain the activity recovery of the catalysts, which display a drop in the methane oxidation, and the production of CO (and H_2 is not observed in the chromatograms). Furthermore, the 12wt% Ni 25% coated surface with Pd displays the best activity on methane total oxidation (Fig.4.15) and no oscillation in the methane conversion. These good properties can result from the Pd which is both very active on methane oxidation and may protect the Ni from deactivation.

$$C_{(s)} + O_{2(g)} = CO_{2(g)} \qquad \Delta H°_{800K} = -394.5\ kJ/mol \quad [4.2]$$

$$C_{(s)} + CO_{2(g)} = 2CO_{(g)} \qquad \Delta H°_{800K} = 172.5\ kJ/mol \quad [4.3]$$

In another hand, the deactivation of the catalyst can occur by the sintering of cobalt. Indeed, blue/light purple particles are observed when inspected the catalytic bed of 12Co, 3Ni-9Co,

2.5Ni-2.5Co, 5Co (just the top of the catalyst bed), 1.5Ni-3.5Co, and 6Ni-14Co (when diluted 10 times in alumina) at the end of methane combustion experiments. These coloured particles are assumed to be sintering cobalt (II) oxide with alumina $CoAl_2O_4$ and indicate a modification of the catalyst during this step. However, literature[41] shows that this cobalt alumina mixed oxide is formed above 1000°C. Nevertheless, it is explained that inactive cobalt alumina mixed oxides can be formed from unreduced cobalt oxide and hydrated alumina, because the presence of water enhances diffusion of small CoO particles[41]. Therefore, this sintering process is favoured by high temperature and steam; conditions in which the tested catalysts are exposed during methane combustion.

5. CONCLUSION

The bimetallic Ni-Co mixed oxide catalysts display good performance on methane combustion, even at low metal loading. However, their performance is not as good as catalysts containing noble metal such as Pd. Moreover, investigation of these materials by UV-Vis spectroscopy shows that they can be unstable during the reaction according to the reaction temperature, result that is confirmed by the oscillation in the calculated methane conversion, active phase oxidized surface and by the production of CO. The phenomena occurring during combustion experiments for low metal loading catalysts (5 and 12wt%) can be explained by a cyclic oxidation/reduction process and/or deactivation of the catalyst by coke formation or sintering when CoO is formed. Therefore, it is recommended to investigate the reactions occurring at the surface of the catalysts in order to get more information about the active phase for combustion (oxide or metallic phase), surface reactivity and avoid oscillation in the methane conversion, which can be prejudicial for the kinetic study. The UV-Vis spectroscopy can be an interesting tool to use for this purpose if coupled with other techniques such as XPS, IR, Raman spectroscopy. A solution should be to work with high metal loading catalysts such as 9Ni-21Co mixed oxide, which displays good performance and stability (according to the combustion temperature). However, in the economic and environmental context high metal loading is not a viable option for the development of a compact reformer. Another alternative to improve the stability of the Ni-Co catalysts is to use promoters. For example, chromium is known for preventing nickel sintering[11] and ceria CeO_2 stabilizes the dispersion of cobalt. Finally, the composition of the catalysts was not as expected. Indeed, it is observed a small loss of magnesium during the preparation, which can explain that the metal loading, is higher than expected. Then, the presence of relatively high amount of Cu and Zn in the compounds can explained the loss of Mg as they can be inserted in the hydrotalcite structure[11]. Therefore, the influence of these elements should also be investigated, because hydrotalcite containing Cu and Zn are active in CO oxidation, methanol production and hydrogenation reactions[11]. To conclude, the textural parameters, and surface activity should be taken into consideration before accurately studying the kinetic of methane combustion over these bimetallic Ni-Co mixed oxides derived from hydrotalcite precursors.

REFERENCES

1. Iulianelli, A.; Liguori, S.; Wilcox, J.; Basile, A. Advances on Methane Steam Reforming to Produce Hydrogen through Membrane Reactors Technology: A Review. Catalysis Reviews 2016, 58 (1), 1–35.

2. Kamiuchi, N.; Eguchi, K. Catalytic Combustion of Methane. In Catalysis for alternative energy generation; New York, 2012; pp 305–327.

3. Semenov, N. N.; Bradley, J. E. S. Some Problems in Chemical Kinetics and Reactivity. Volume 2; 1959.

4. Lee, J. H.; Trimm, D. L. Catalytic Combustion of Methane. Fuel Processing Technology 1995, 42 (2–3), 339–359.

5. Jiang, Z.; Hao, Z.; Yu, J.; Hou, H.; Hu, C.; Su, J. Catalytic Combustion of Methane on Novel Catalysts Derived from Cu-Mg/Al-Hydrotalcites. Catalysis Letters 2005, 99 (3–4), 157–163.

6. Liotta, L.; Dicarlo, G.; Pantaleo, G.; Deganello, G. CoO/CeO and CoO/CeO–ZrO Composite Catalysts for Methane Combustion: Correlation between Morphology Reduction Properties and Catalytic Activity. Catalysis Communications 2005, 6 (5), 329–336.

7. Li, Z.; Hoflund, G. B. Catalytic Oxidation of Methane over Pd/Co3O4. Reaction Kinetics and Catalysis Letters 1999, 66 (2), 367–374.

8. Lim, T. H.; Cho, S. J.; Yang, H. S.; Engelhard, M.; Kim, D. H. Effect of Co/Ni Ratios in Cobalt Nickel Mixed Oxide Catalysts on Methane Combustion. Applied Catalysis A: General 2015, 505, 62–69.

9. Arai, H.; Yamada, T.; Eguchi, K.; Seiyama, T. Catalytic Combustion of Methane over Various Perovskite-Type Oxides. Applied Catalysis 1986, 26, 265–276.

10. Marchetti, L.; Forni, L. Catalytic Combustion of Methane over Perovskites. Appl. Catal. B 1998, 15, 179–187.

11. Cavani, F.; Trifiró, F.; Vaccari, A. Hydrotalcite-Type Anionic Clays: Preparation, Properties and Applications; Catalysis today; Elsevier, 1991.

12. Jiang, Z.; Yu, J.; Cheng, J.; Xiao, T.; Jones, M. O.; Hao, Z.; Edwards, P. P. Catalytic Combustion of Methane over Mixed Oxides Derived from Co–Mg/Al Ternary Hydrotalcites. Fuel Processing Technology 2010, 91 (1), 97–102.

13. Khassin, A. A.; Yurieva, T. M.; Kustova, G. N.; Itenberg, I. S.; Demeshkina, M. P.; Krieger, T. A.; Plyasova, L. M.; Chermashentseva, G. K.; Parmon, V. N. Cobalt–aluminum Co-Precipitated Catalysts and Their Performance in the Fischer–Tropsch Synthesis. Journal of Molecular Catalysis A: Chemical 2001, 168 (1–2), 193–207.

14. Chmielarz, L.; Kuśtrowski, P.; Rafalska-Łasocha, A.; Majda, D.; Dziembaj, R. Catalytic Activity of Co-Mg-Al, Cu-Mg-Al and Cu-Co-Mg-Al Mixed Oxides Derived from Hydrotalcites in SCR of NO with Ammonia. Applied Catalysis B: Environmental 2002, 35 (3), 195–210.

15. Yu, J. J.; Cheng, J.; Ma, C. Y.; Wang, H. L.; Li, L. D.; Hao, Z. P.; Xu, Z. P. NOx Decomposition, Storage and Reduction over Novel Mixed Oxide Catalysts Derived from Hydrotalcite-like Compounds. Journal of Colloid and Interface Science 2009, 333 (2), 423–430.

16. Zanfir, M.; Gavriilidis, A. Catalytic Combustion Assisted Methane Steam Reforming in a Catalytic Plate Reactor. Chemical Engineering Science 2003, 58 (17), 3947–3960.

17. Agar, D. W. Multifunctional Reactors: Old Preconceptions and New Dimensions. Chemical Engineering Science 1999, 54 (10), 1299–1305.

18. Ridler, D. E.; Twigg, M. V. Catalyst Handbook, Wolf Publishing Ltd.; London, 1989.

19. Irankhah, A.; Rahimi, M.; Rezaei, M. Performance Research on a Methane Compact Reformer Integrated with Catalytic Combustion. Chemical Engineering & Technology 2014, 37 (7), 1220–1226.

20. Crystal Structure Analysis: Principles and Practice, 2nd ed.; Blake, A. J., Clegg, W., Eds.; International Union of Crystallography book series; Oxford University Press: Oxford ; New York, 2009.

21. Ebsworth, E. A. V.; Rankin, D. W. H.; Cradock, S. Structural Methods in Inorganic Chemistry, 2nd ed.; CRC Press: Boca Raton, Fla, 1991.

22. Thomas, J. M.; Thomas, W. J. Principles and Practice of Heterogeneous Catalysis; VCH: Weinheim ; New York, 1997.

23. Sing, K. S. W. Reporting Physisorption Data for Gas/Solid Systems with Special Reference to the Determination of Surface Area and Porosity (Recommendations 1984). Pure and Applied Chemistry 1985, 57 (4).

24. Brunauer, S.; Emmett, P. H.; Teller, E. Adsorption of Gases in Multimolecular Layers. Journal of the American Chemical Society 1938, 60 (2), 309–319.

25. Williams, D. B.; Carter, C. B. Transmission Electron Microscopy:: A Textbook for Materials Science. Pt.1 Basics, 2. ed.; Springer: New York, 2009.

26. Goldstein, J. I.; Newbury, D. E.; Echlin, P.; Joy, D. C.; Lyman, C. E.; Lifshin, E.; Sawyer, L.; Michael, J. R. Scanning Electron Microscopy and X-Ray Microanalysis; 2013.

27. Gas Chromatography: A Practical Approach; Baugh, P. J., Ed.; The Practical approach series; IRL Press at Oxford University Press: Oxford ; New York, 1993.

28. Li, H. Sorption Enhanced Steam Reforming of Biomass-Derived Compounds: Process and Material. PhD thesis, Norwegian University of Science and Technology, 2010.

29. Mul, G.; Moulijn, J. A. Preparation of Supported Metal Catalysts. ChemInform 2005, 36 (45).

30. Ferreira, B. D. L.; Paulo, J. M.; Braga, J. P.; Sebastião, R. C. O.; Pujatti, F. J. P. Methane Combustion Kinetic Rate Constants Determination: An Ill-Posed Inverse Problem Analysis. Química Nova 2013, 36 (2), 262–266.

31. Westbrook, C. K.; Dryer, F. L. Simplified Reaction Mechanisms for the Oxidation of Hydrocarbon Fuels in Flames. Combustion Science and Technology 1981, 27 (1–2), 31–43.

32. Westbrook, C. K.; Dryer, F. L. Chemical Kinetic Modelling of Hydrocarbon Combustion. Progress in Energy and Combustion Science 1984, 10 (1), 1–57.

33. Kortüm, G. Reflectance Spectroscopy; Springer Berlin Heidelberg: Berlin, Heidelberg, 1969.

34. Nagano, T.; Nakashima, S. Study of Colors and Degrees of Weathering of Granitic Rocks by Visible Diffuse Reflectance Spectroscopy. GEOCHEMICAL JOURNAL 1989, 23 (2), 75–83.

35. Perkampus, H.-H. Recent Developments in UV-VIS Spectroscopy. In UV-VIS Spectroscopy and Its Applications; Springer Berlin Heidelberg: Berlin, Heidelberg, 1992; pp 81–130.

36. Lietz, G. Reactions of Platinum in Oxygen- and Hydrogen-Treated Pt/gamma-Al2O3 Catalysts II. Ultraviolet-Visible Studies, Sintering of Platinum, and Soluble Platinum. Journal of Catalysis 1983, 81 (1), 17–25.

37. Zhang, X.; Lee, C.; Hayward, D.; Mingos, D. Oscillatory Behaviour Observed in the Rate of Oxidation of Methane over Metal Catalysts. Catalysis Today 2005, 105 (2), 283–294.

38. Guisnet, M.; Magnoux, P. Organic Chemistry of Coke Formation. Applied Catalysis A: General 2001, 212 (1–2), 83–96.

39. Alenazey, F.; Cooper, C.; Dave, C.; Elnashaie, S.; Susu, A.; Adesina, A. Coke Removal from Deactivated Co–Ni Steam Reforming Catalyst Using Different Gasifying Agents: An Analysis of the Gas–solid Reaction Kinetics. Catalysis Communications 2009, 10 (4), 406–411.

40. Figueiredo, J. Gasification of Carbon Deposits on Catalysts and Metal Surfaces. Fuel 1986, 65 (10), 1377–1382.

41. The Role of Catalysis for the Sustainable Production of Bio-Fuels and Bio-Chemicals, 1st ed.; Triantafyllidis, K. S., Lappas, A. A., Stöcker, M., Eds.; Elsevier: Amsterdam; Boston, 2013.

42. Reddy, B. M.; Rao, K. N.; Bharali, P. Copper Promoted Cobalt and Nickel Catalysts Supported on Ceria−Alumina Mixed Oxide: Structural Characterization and CO Oxidation Activity. Industrial & Engineering Chemistry Research 2009, 48 (18), 8478–8486.

43. Wei, L.; Geng, P. A Review on Natural Gas/Diesel Dual Fuel Combustion, Emissions and Performance. Fuel Processing Technology 2016, 142, 264–278.

44. Li, Z.; Hoflund, G. B. A Review on Complete Oxidation of Methane at Low Temperatures. 2003, 12 (3), 153–160.

45. Wu, H.; La Parola, V.; Pantaleo, G.; Puleo, F.; Venezia, A.; Liotta, L. Ni-Based Catalysts for Low Temperature Methane Steam Reforming: Recent Results on Ni-Au and Comparison with Other Bi-Metallic Systems. Catalysts 2013, 3 (2), 563–583.

46. Ni, M. 2D Heat and Mass Transfer Modeling of Methane Steam Reforming for Hydrogen Production in a Compact Reformer. Energy Conversion and Management 2013, 65, 155–163.

47. Khoshandam, B.; Jamshidi, E.; Kumar, R. V. Reduction of Cobalt Oxide with Methane. Metallurgical and Materials Transactions B 2004, 35 (5), 825–828.

48. Yousaf, B. Hydrotalcite Based Ni-Co Bi-Metallic Catalysts for Steam Reforming of Methane. Master thesis, Norwegian University of Science and Technology: Trondheim, 2016.

49. Corbo, P.; Migliardini, F. Hydrogen Production by Catalytic Partial Oxidation of Methane and Propane on Ni and Pt Catalysts. International Journal of Hydrogen Energy 2007, 32 (1), 55–66.

APPENDIX

A. Calculations for the preparation and the composition of the catalysts

The estimated composition of the the Ni-Co/MgO/Al_2O_3 catalyst are calculated as follow. With q= mol Co^{2+} , x= mol Ni^{2+} , y= mol MgO and z= mol Al_2O_3

$$\frac{z}{q+x+y+z} = 0.25 \qquad [B.1]$$

For 1mol Al^{3+}, z=1

The relation [B.1] becomes $q + x + y = 3 \Rightarrow$ $\boxed{y = 3 - q - x}$ [B.2]

The weight fraction of Ni (w_{Ni}) and Co (w_{Co}) are:

$$w_{Ni} = \frac{m_{Ni}}{m_{Ni}+m_{Co}+m_{MgO}+m_{Al2O3}} = \frac{x.M_{Ni}}{x.M_{Ni}+q.M_{Co}+y.M_{MgO}+M_{Al2O3}} \qquad [B.3]$$

$$w_{Co} = \frac{m_{Co}}{m_{Ni}+m_{Co}+m_{MgO}+m_{Al2O3}} = \frac{q.M_{Co}}{x.M_{Ni}+q.M_{Co}+y.M_{MgO}+M_{Al2O3}} \qquad [B.4]$$

Then by inserting the relation [2] in [3], the equation [5] for the Ni amount is obtained

$$\boxed{x = \frac{w_{Ni}(q.M_{Co}-q.M_{MgO}+3M_{MgO}+0.5M_{Al2O3})}{(1-w_{Ni}).M_{Ni}+w_{Ni}.M_{MgO}}} \qquad [B.5]$$

By inserting [2] and [5] in [4], the equation [6] for the Co amount is obtained

$$\boxed{q = \frac{3M_{MgO}+0.5M_{Al2O3}}{\frac{M_{Co}}{w_{Co}}\left[(1-w_{Ni})+w_{Ni}.\frac{M_{MgO}}{M_{Ni}}\right]-M_{Co}+M_{MgO}}} \qquad [B.6]$$

Therefore, the molar composition of the materials is given in table 1.

Table 1: Estimation of the molar composition of the prepared mixed oxide catalysts derived from hydrotalcite precursors.

Metal Loading [%]		Mass fractions		q	x	y	z
Ni	Co	W_{Ni}	W_{Co}				
2,5	2,5	0,025	0,025	0,07	0,07	2,85	1
1,5	3,5	0,015	0,035	0,10	0,04	2,85	1
3,5	1,5	0,035	0,015	0,04	0,10	2,85	1
5	0	0,05	0	0	0,16	2,85	1
0	5	0	0,05	0,15	0	2,85	1

As Al_2O_3 contains two Al^{3+} ions, the stoichiometric coefficients of the materials component are calculated and shown in table 2.

Table 2: Stoichiometric coefficients of the ions constituting the prepared hydrotalcite based compounds.

Catalyst	Stoichiometric coefficients					
	Ni^{+2}	Co^{+2}	Mg^{+2}	Al^{+3}	OH^-	CO_3^{-2}
2.5Ni-2.5Co	0,15	0,15	5,70	2,00	16,00	1
1.5Ni-3.5Co	0,09	0,21	5,70	2,00	16,00	1
3.5Ni-1.5Co	0,21	0,09	5,70	2,00	16,00	1
5Ni	0,30	0,00	5,70	2,00	16,00	1
5Co	0,00	0,30	5,70	2,00	16,00	1

Therefore, the estimated formulas of the prepared catalysts are shown in table 3.

Table 3: General formulas of the prepared hydrotalcite based materials.

Catalyst	Formula
2.5Ni-2.5Co	$Ni_{0.15}\ Co_{0.15}Mg_{5.7}\ Al_2\ (OH)_{16}]^{2+}.(CO_3^{2-}).mH_2O$
1.5Ni-3.5Co	$[Ni_{0.09}\ Co_{0.21}Mg_{5.7}\ Al_2\ (OH)_{16}]^{2+}.(CO_3^{2-}).mH_2O$
3.5Ni-1.5Co	$[Ni_{0.21}\ Co_{0.09}Mg_{5.7}\ Al_2\ (OH)_{16}]^{2+}.(CO_3^{2-}).mH_2O$
5Ni	$[Ni_{0.3}Mg_{5.7}\ Al_2\ (OH)_{16}]^{2+}.(CO_3^{2-}).mH_2O$
5Co	$[Co_{0.3}Mg_{5.7}\ Al_2\ (OH)_{16}]^{2+}.(CO_3^{2-}).mH_2O$

Finally, in order to have the following carbonate to aluminium ratio in the final materials, the amount of reactants were calculated on the basis of $n_{CO3^{2-}} = 0.0375$ mol (therefore for $n_{Al3+} = 0{,}075$ mol) and shown in table 4. Moreover, Cavani[11] emphasized that carbonate amount should be introduced in slight excess in the reaction mixture.

$$\frac{n_{CO3^{2-}}}{n_{Al3+}} = 0.5$$

Table 4: Mass of the reactants used for the hydrotalcite based compounds.

Catalysts	**Mass of the Reactants (g)**					
	$Ni(NO_3)_2.6H_2O$	$Co(NO_3)_2.6H_2O$	$Mg(NO_3)_2.6H_2O$	$Al(NO_3)_3.9H_2O$	NaOH	Na_2Co_3
2.5Ni-2.5Co	1,62	1,62	54,83	28,13	24,00	5,96
1.5Ni-3.5Co	0,97	2,26	54,84	28,13	24,00	5,96
3.5Ni-1.5Co	2,27	0,97	54,83	28,13	24,00	5,96
5Ni	3,24	0,00	54,84	28,13	24,00	5,96
5Co	0,00	3,23	54,84	28,13	24,00	5,96

B. Aspect of the catalysts

Picture 1: On top: The prepared 5wt% Ni-Co hydrotalcite precursors, from left to right: 3.5Ni-1.5Co HT, 2.5Ni-2.5Co HT, 1.5Ni-3.5Co HT and 5Co HT. To the bottom: the mixed oxide catalysts derived from these hydrotalcite precursors after the treatment at 600°C for 6h. From left to right: 5Ni, 3.5Ni-1.5Co, 2.5Ni-2.5Co, 1.5Ni-3.5Co and 5Co mixed oxides.

Picture 2: 12wt%Co mixed oxide catalyst diluted in Al_2O_3 after methane combustion.

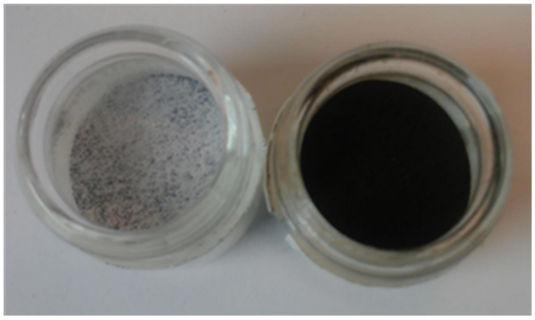

Picture 3: Left: 12wt% Co catalyst diluted in Al_2O_3 after methane combustion (blue particles in white alumina powder. Right: 12wt% Co mixed oxide catalyst.

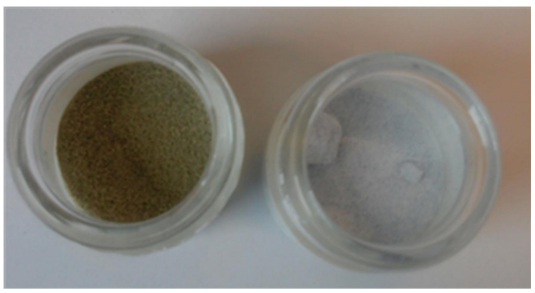

Picture 4: Left: 1.5Ni-3.5 Co catalyst. Right: 1.5Ni-3.5Co catalyst diluted in Al_2O_3 after methane combustion (purple particles in white alumina powder).

C. Gas chromatographs

The Fig.1C shows the shape of integrated peaks used for methane conversion calculation. The, the Fig.1D shows the shapes of unknown peaks which are called “noises” and which do not permit to calculate the methane conversion over some tested catalysts (for instance 5Ni and 6Ni-6Co) and at low temperatures (below 400°C°).

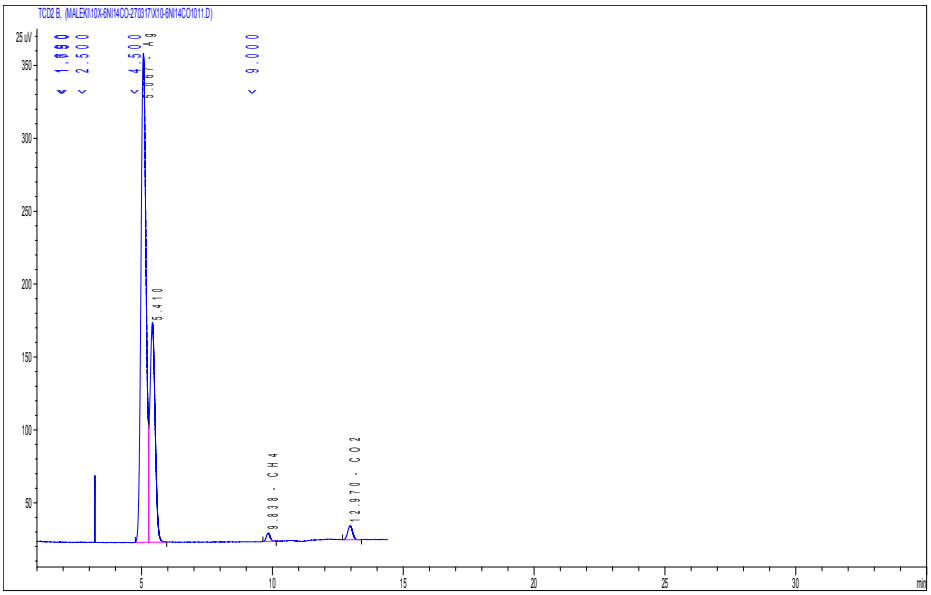

Fig.1C: Chromatogram of the gas mixture during the methane combustion over 6Ni-14Co mixed oxide catalyst at 700°C. The chromatograph shows peaks of Ar (5,06min), O_2/N_2(5,41min), CH_4 (9,82 min) and CO_2 (12,97 min)

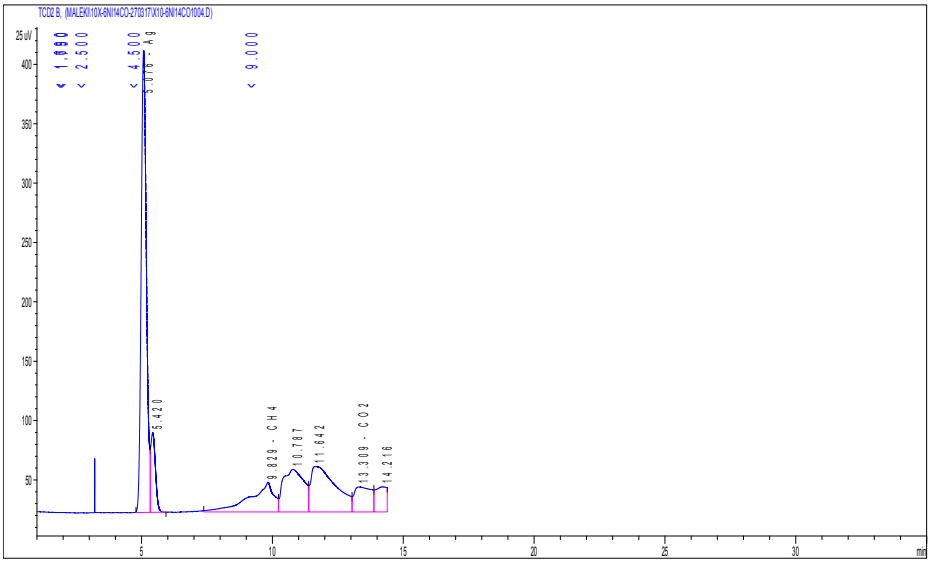

Fig. 2C: Chromatogram of the gas mixture during the methane combustion over 6Ni-14Co mixed oxide catalyst at 400°C. It shows unknown peaks, which are called “noises”, making the integration of the peaks not accurate.

D. Calibration of the mass flow controllers

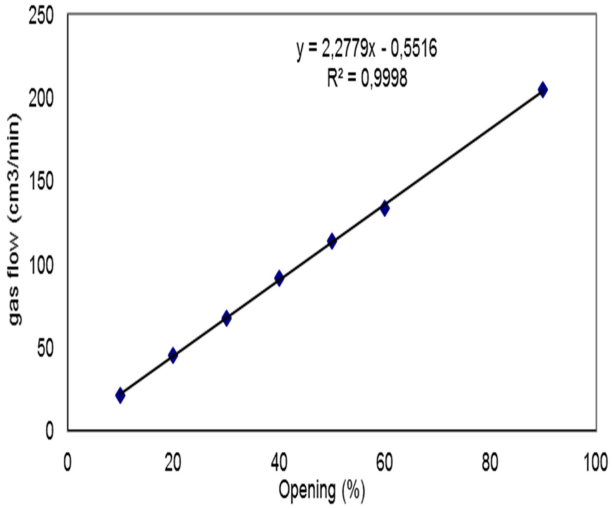

Fig. D.1: Ar flow as a function of the gas opening.

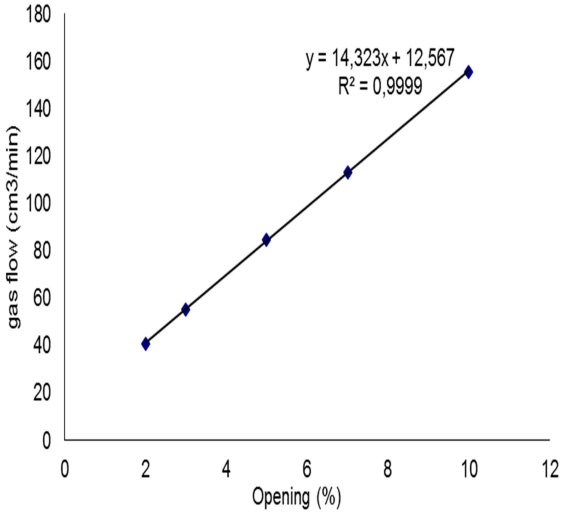

Fig. D.2: H_2 flow as a function of the gas opening.

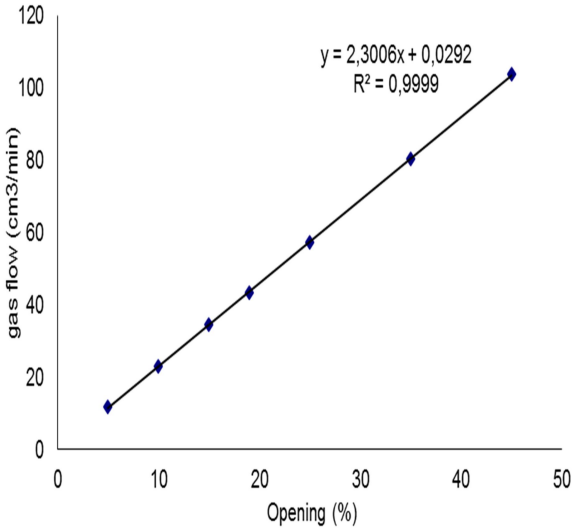

Fig. D.3: Air flow as a function of the gas opening.

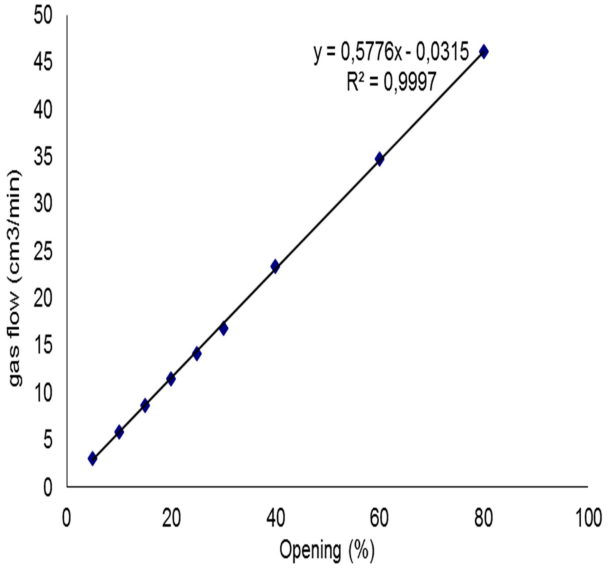

Fig D.4: CH_4 flow as a function of the gas opening.

E. UV-Vis reflectance curves of the Ni-Co mixed oxide catalysts

E.A. 5wt% Ni-Co catalysts

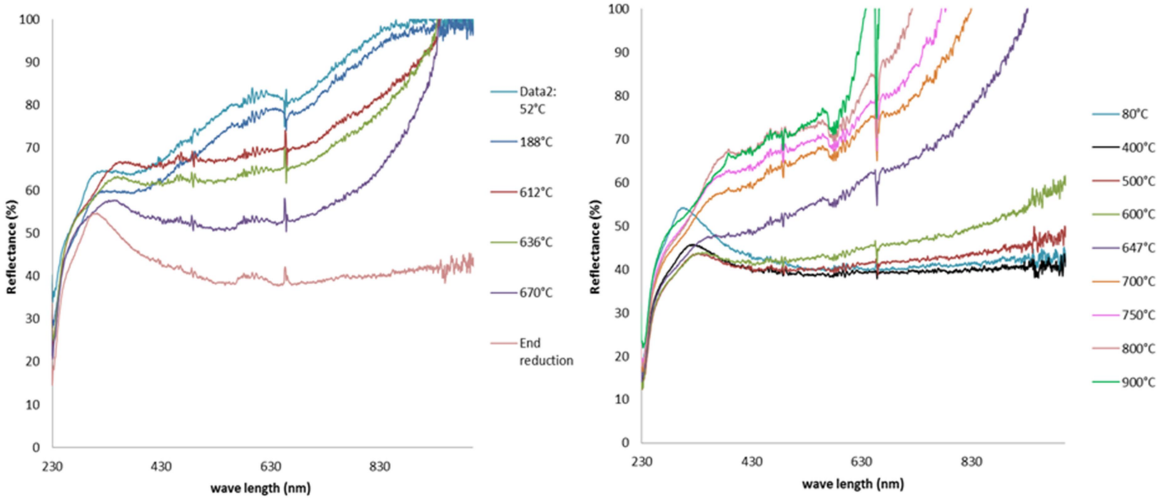

Fig E.1: UV-Vis spectra of the 2.5Ni-2.5Co mixed oxide catalyst during reduction (left) and methane combustion (right) steps at different furnace temperatures.

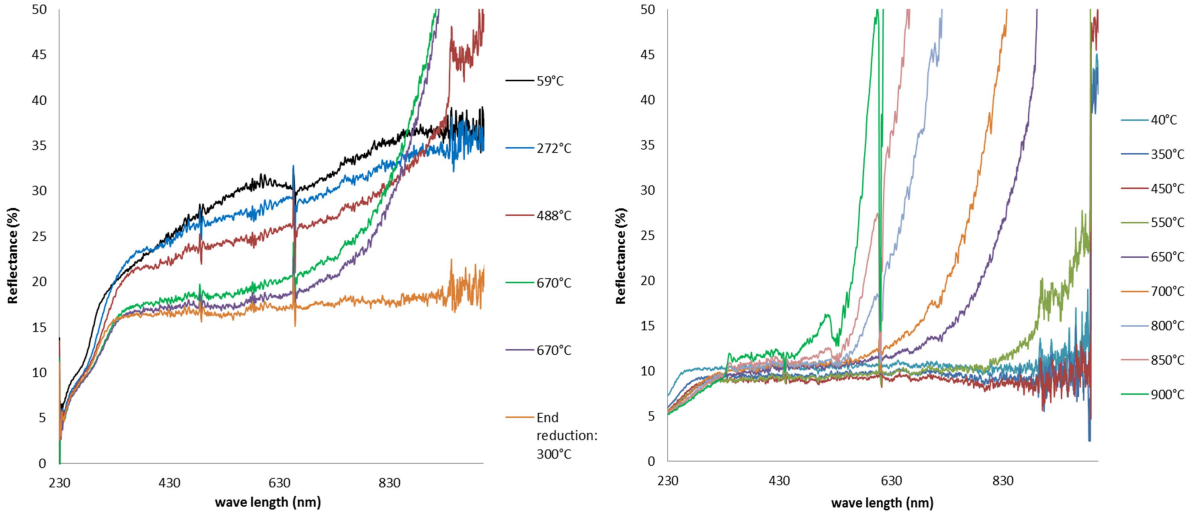

Fig E.2: UV-Vis spectra of the 3.5Ni-1.5Co mixed oxide catalyst during reduction (left) and methane combustion (right) steps at different furnace temperatures. The reflectance curves during the combustion are not as expected; it might be cause by a problem in the experimental set-up. Nevertheless, the low intensities of reflectance even at high temperature show that this material is less oxidized. Moreover, it is the catalyst displaying the lowest methane conversion. Therefore, it shows that a certain amount of oxidized phase is required in order to achieve high methane conversion.

E.B. 12wt% Ni-Co catalysts

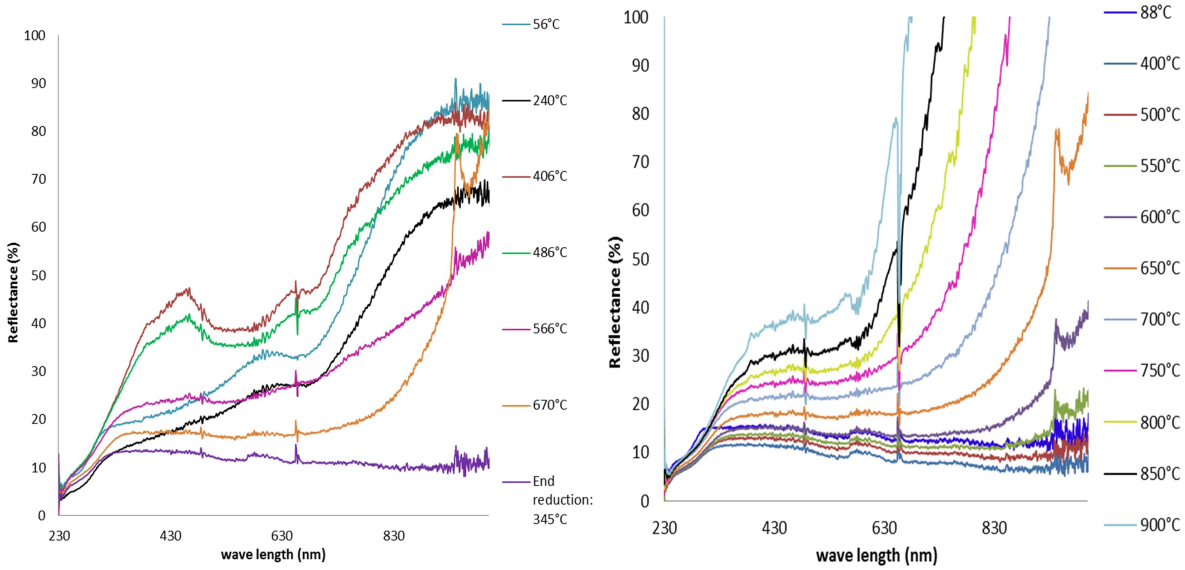

Fig E.3: UV-Vis spectra of the 3Ni-9Co mixed oxide catalyst during reduction (left) and methane combustion (right) steps at different furnace temperatures.

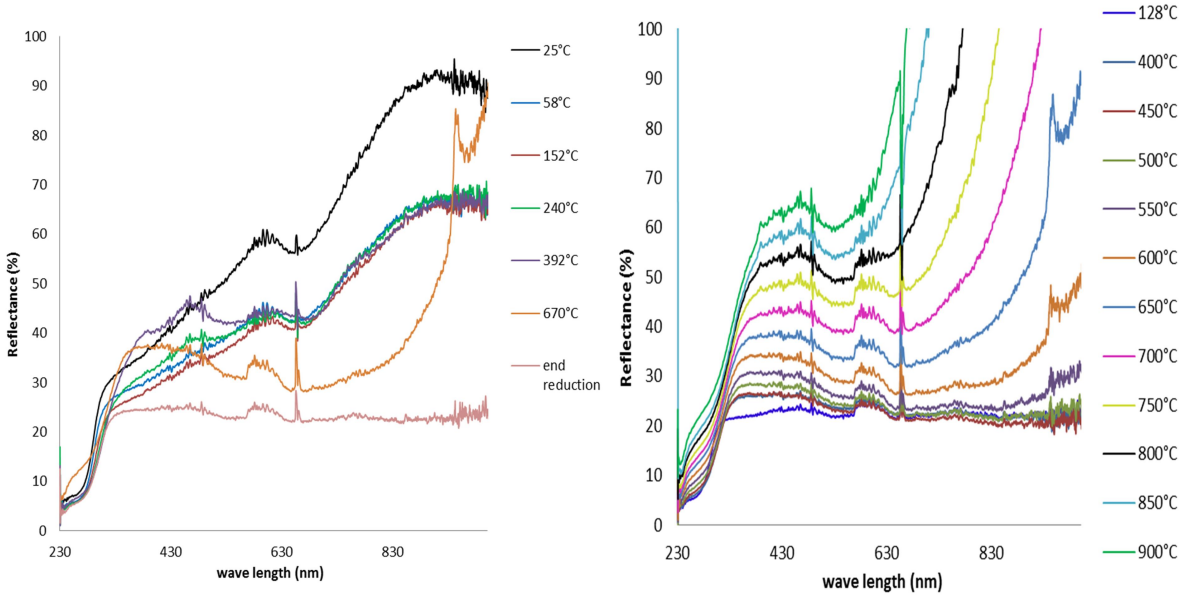

Fig E.4: UV-Vis spectra of the 6Ni-6Co mixed oxide catalyst during reduction (left) and methane combustion (right) steps at different furnace temperatures.

E.C 20 and 30wt% Ni-Co catalysts

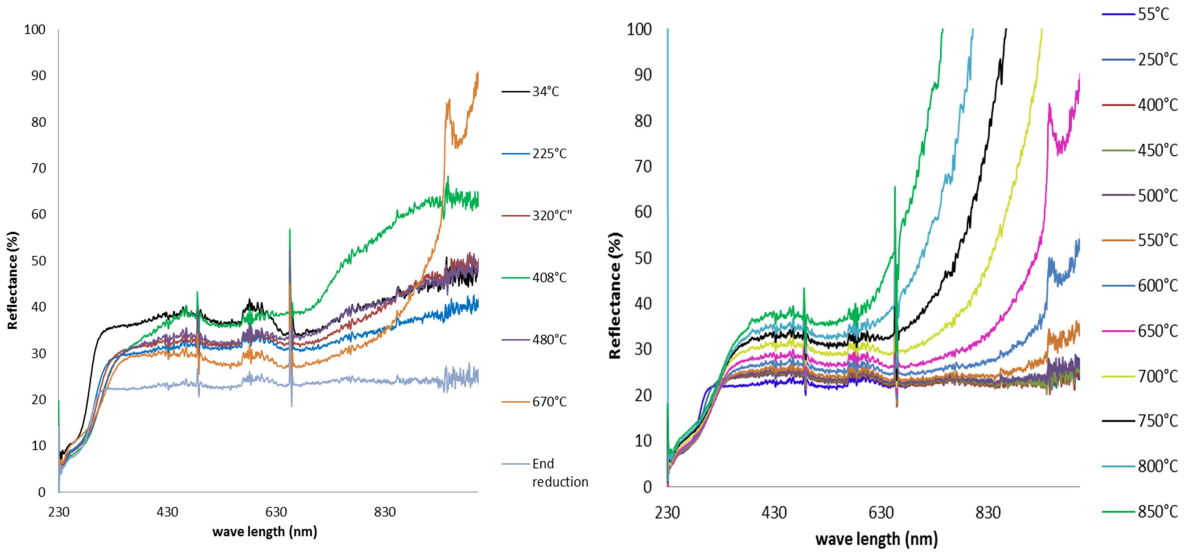

Fig E.5: UV-Vis spectra of the 6Ni-14Co mixed oxide catalyst during reduction (left) and methane combustion (right) steps at different furnace temperatures.

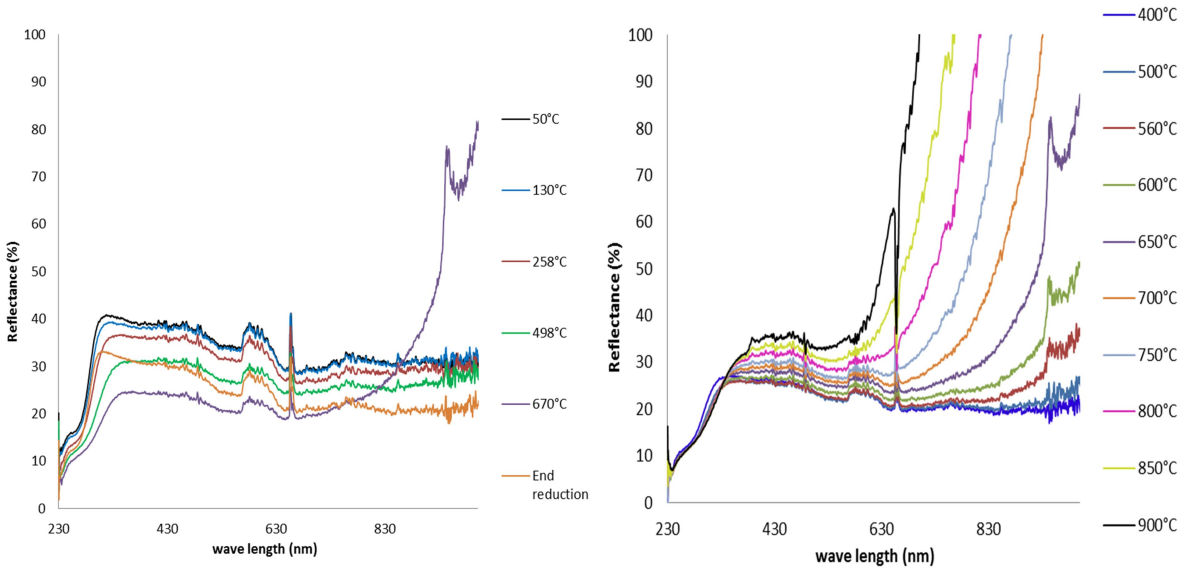

Fig E.6: UV-Vis spectra of the 9Ni-21Co mixed oxide catalyst during reduction (left) and methane combustion (right) steps at different furnace temperatures.

F. Estimation of the oxidation fraction of the catalysts

Relation [F.1] is used in order to calculate the fraction of oxidized surface during the reduction of the catalyst based on the UV-Vis reflectance curves of the catalysts.

$$S_{ox} = \frac{R_t - R_\infty}{R_o - R_\infty} \qquad [F.1]$$

Where R_t is the intensity of reflectance at a specific temperature, R_o is the intensity of reflectance at the beginning of the reduction R_∞ is the intensity of reflectance at the end of the reduction.

The relation above is only used for the 5Ni catalysts with the intensities reflectance at λ=589.3nm, see Fig.F.1. Indeed, the reflectance curves of the Co and bimetallic Ni-Co catalysts present two tendencies, which are interpreted as Co^{3+} to Co^{2+} transition followed by the Co^{2+} to Co^0 transition during the reduction of these catalysts. Therefore, the estimation of the oxidized fraction of the cobalt is more complex and requires assumptions, which do not permit to calculate it with the relation [F.1].

An estimation of the fraction of oxidized surface on the tested catalysts during methane combustion was calculated according to the relation [F.2] which is based on the intensities of reflectance at λ= 430,5nm. This wavelength was chosen because reflectance intensities do not display large deviation due to the furnace temperature and the feature (oscillation in the reflectance) attributed to cobalt are also observed. Moreover, it is assumed that the active phase is totally reduced at the beginning of the combustion and totally oxidized at a combustion temperature of 900°C (which means we did not consider the state of cobalt).

$$S_{ox} = \frac{R_t - R_o}{R_\infty - R_o} \qquad [F.2]$$

Where R_t is the intensity of reflectance at a specific temperature, R_o is the intensity of reflectance at the beginning of the methane combustion (low temperature), R_∞ is the intensity of reflectance at the end of the combustion (at 900°C).

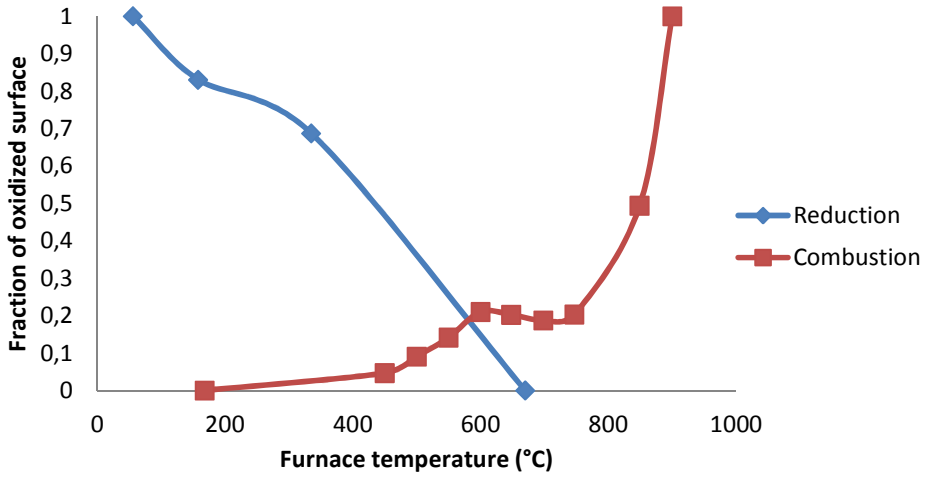

Fig F.1: UV-Vis spectra of the 3.5Ni-1.5Co mixed oxide catalyst during reduction (left) and methane combustion (right) steps at different furnace temperatures

ID	16925	**Status**	**Date**
Risk Area	Risikovurdering: Helse, miljø og sikkerhet (HMS)	Created	02.02.2017
Created by	Hilde Apneseth	Assessment started	02.02.2017
Responsible	Hilde Apneseth	Actions decided	
		Closed	

Risk Assessment:

CAT, Exchange student, 2017, Leyman Maleki Bakali-Hemou

Valid from-to date:

1/23/2017 - 6/30/2017

Location:

Catalysis group

Goal / purpose

Risk assessment for the synthesis and analysis that will be performed during my master thesis in the Catalysis group under the supervision of Pr. De Chen. The task consists mainly on the kinetic study of methane combustion in quartz fixed bed reactor, with Ni-Co based catalysts. These catalysts will be prepared by co-precipitation method and characterized by using various techniques such as BET, H2 chimisorption, XRF, XRD, SEM-XEDS

Background

BET, H2 chemisorption, XRF, XRD, SEM, furnaces
method: catalyst synthesis by co-precipitation
chemicals: Co(NO3)2. 6H2O; Ni(NO3)2.6H2O; Mg(NO3)2.6H2O ; Al(NO3)3.9H2O ; NaOH ; Na2CO3

Description and limitations

No specific risks by using magnesium (II) and aluminium (III) nitrate

Prerequesites, assumptions and simplifications

NaOH and Na2CO3 are corrosives
X-ray exposure may occurs by using XRF and XRD
Be careful with liquid N2 for BET analysis
toxicity of Ni and Co precursors
Burns from the reactor furnace at high temperature

Attachments

productCo.pdf
productNi.pdf
productMg.pdf

References

[Ingen registreringer]

Summary, result and final evaluation

The summary presents an overview of hazards and incidents, in addtition to risk result for each consequence area.

Hazard:	**N2 adsorption analysis (BET)**		
Incident:	**contact with liquid nitrogen (N2)**		
Consequence area:	Helse	Risk before actions:	Risiko after actions:
Hazard:	**Synthesis by co-precipitation method**		
Incident:	**To be in contact with cobalt (II) nitrate**		
Consequence area:	Helse	Risk before actions:	Risiko after actions:
	Ytre miljø	Risk before actions:	Risiko after actions:
Incident:	**To be in contact of Nickel (II) nitrate**		
Consequence area:	Helse	Risk before actions:	Risiko after actions:
	Ytre miljø	Risk before actions:	Risiko after actions:
Incident:	**Contact with sodium hydroxide (NaOH) and Na2(CO3)**		
Consequence area:	Helse	Risk before actions:	Risiko after actions:
Hazard:	**X-ray exposure when using XRD and XRF**		
Incident:	**irradiation by X-ray**		
Consequence area:	Helse	Risk before actions:	Risiko after actions:
Hazard:	**calcination furnace**		
Incident:	**skin burns**		
Consequence area:	Helse	Risk before actions:	Risiko after actions:

Hazard:	**calcination furnace**
Incident:	**furnace explosure**

Consequence area: Helse — Risk before actions: [x] Risiko after actions: [x]

Hazard:	**Methane oxidation reactor**
Incident:	**Explosion due to flammable gas such as hydrogen and methane**

Consequence area: Helse — Risk before actions: [x] Risiko after actions: [x]

Materielle verdier — Risk before actions: [x] Risiko after actions: [x]

Incident: **Burns**

Consequence area: Helse — Risk before actions: [x] Risiko after actions: [x]

Final evaluation

Organizational units and people involved

A risk assessment may apply to one or more organizational units, and involve several people. These are lsited below.

Organizational units which this risk assessment applies to

- Institutt for kjemisk prosessteknologi

Participants

De Chen
Shirley Elisabeth Liland
Karin Wiggen Dragsten
Gunn Torill Wikdahl
Kumar Ranjan Rout
Leyman Maleki Bakali-Hemou

Readers

[Ingen registreringer]

Others involved/stakeholders

[Ingen registreringer]

The following accept criteria have been decided for the risk area Risikovurdering: Helse, miljø og sikkerhet (HMS):

Helse	Materielle verdier	Omdømme	Ytre miljø

Overview of existing relevant measures which have been taken into account

The table below presents existing measures which have been take into account when assessing the likelihood and consequence of relevant incidents.

Hazard	Incident	Measures taken into account
N2 adsorption analysis (BET)	contact with liquid nitrogen (N2)	
Synthesis by co-precipitation method	To be in contact with cobalt (II) nitrate	
	To be in contact of Nickel (II) nitrate	
	Contact with sodium hydroxide (NaOH) and Na2(CO3)	
X-ray exposure when using XRD and XRF	irradiation by X-ray	
calcination furnace	skin burns	
	furnace explosure	
Methane oxidation reactor	Explosion due to flammable gas such as hydrogen and methane	ventillation
	Explosion due to flammable gas such as hydrogen and methane	Apparatus located inside a closed glass box
	Burns	protective gloves

Existing relevant measures with descriptions:

fume hood with good ventillation

[Ingen registreringer]

protective gloves

[Ingen registreringer]

safety googles

latex or vinyl gloves (according to laboratory and workshop handbook)

lab coat

[Ingen registreringer]

dust mask

[Ingen registreringer]

security system to stop X-ray beamlight

No X-ray production if the experiment is not set up well
X-ray beam stops if there is a problem

isolating gloves

[Ingen registreringer]

ventillation

[Ingen registreringer]

Apparatus located inside a closed glass box

[Ingen registreringer]

system to turn off heat and electricity

[Ingen registreringer]

Risk analysis with evaluation of likelihood and consequence

This part of the report presents detailed documentation of hazards, incidents and causes which have been evaluated. A summary of hazards and associated incidents is listed at the beginning.

The following hazards and incidents has been evaluated in this risk assessment:

- **N2 adsorption analysis (BET)**
  - contact with liquid nitrogen (N2)
- **Synthesis by co-precipitation method**
  - To be in contact with cobalt (II) nitrate
  - To be in contact of Nickel (II) nitrate
  - Contact with sodium hydroxide (NaOH) and Na2(CO3)
- **X-ray exposure when using XRD and XRF**
  - irradiation by X-ray
- **calcination furnace**
  - skin burns
  - furnace explosure
- **Methane oxidation reactor**
  - Explosion due to flammable gas such as hydrogen and methane
  - Burns

Detailed view of hazards and incidents:

Hazard: N2 adsorption analysis (BET)

Incident: contact with liquid nitrogen (N2)

Cause: Not wearing the appropriate safety equipments

Description:
isolating gloves, lab coat, safety googles, gloves, closed shoes

Likelihood of the incident (common to all consequence areas): **Unlikely (1)**

Kommentar:
always wear the safety equipment

Consequence area: Helse ***Risk:***

Assessed consequence: **Small (1)**

Comment: [Ingen registreringer]

Hazard: Synthesis by co-precipitation method

Incident: To be in contact with cobalt (II) nitrate

chemical that is carcinogenic, harmful to DNA and environment

Cause: Not enough or no ventillation in the fume hood

Likelihood of the incident (common to all consequence areas): **Less likely (2)**

Kommentar:

[Ingen registreringer]

Consequence area: Helse ***Risk:***

Assessed consequence: **Very large (4)**

Comment: carcinogenic and harmful to DNA product

Consequence area: Ytre miljø ***Risk:***

Assessed consequence: **Small (1)**

Comment: [Ingen registreringer]

Incident: To be in contact of Nickel (II) nitrate

chemical that is carcinogenic, harmful to DNA and environment

Cause: Not enough or no ventillation in the fume hood

Cause: Not appropriate protective gloves

Likelihood of the incident (common to all consequence areas): **Likely (3)**

Kommentar:

[Ingen registreringer]

Consequence area: Helse ***Risk:***

Assessed consequence: **Large (3)**

Comment: corrosive product so can cause skin injuries, it is also carcinogenic and harmful to DNA

Consequence area: Ytre miljø ***Risk:***

Assessed consequence: **Small (1)**

Comment: [Ingen registreringer]

Incident: Contact with sodium hydroxide (NaOH) and Na2(CO3)

corrosive products

Cause: No gloves or Not appropriate gloves

Likelihood of the incident (common to all consequence areas): **Unlikely (1)**

Kommentar:

[Ingen registreringer]

Consequence area: Helse ***Risk:***

Assessed consequence: **Medium (2)**

Comment: [Ingen registreringer]

Hazard: X-ray exposure when using XRD and XRF

when using XRF and XRD

Incident: irradiation by X-ray

Likelihood of the incident (common to all consequence areas): **Unlikely (1)**

Kommentar:

[Ingen registreringer]

Consequence area: Helse ***Risk:***

Assessed consequence: **Very large (4)**

Comment: [Ingen registreringer]

Hazard: calcination furnace

Incident: skin burns

Likelihood of the incident (common to all consequence areas): **Less likely (2)**

Kommentar:

[Ingen registreringer]

Consequence area: Helse ***Risk:***

Assessed consequence: **Medium (2)**

Comment: [Ingen registreringer]

Incident: furnace explosure

Likelihood of the incident (common to all consequence areas): **Unlikely (1)**

Kommentar:

sample amount very low and we avoid putting flammable materials at high temperature

Consequence area: Helse ***Risk:***

Assessed consequence: **Medium (2)**

Comment: If we wear the protective equipment (lab coat, glasses, isolating gloves,...)

Hazard: Methane oxidation reactor

Set-up 2.12 Hall D

Incident: Explosion due to flammable gas such as hydrogen and methane

Cause: hydrogen and methane leaking

Likelihood of the incident (common to all consequence areas): **Unlikely (1)**

Kommentar:

[Ingen registreringer]

Consequence area: Helse ***Risk:***

Assessed consequence: **Small (1)**

Comment: [Ingen registreringer]

Consequence area: Materielle verdier ***Risk:***

Assessed consequence: **Medium (2)**

Comment: [Ingen registreringer]

Incident: Burns

External part of the furnace is hot during the combustion

Likelihood of the incident (common to all consequence areas): **Likely (3)**

Kommentar:

[Ingen registreringer]

Consequence area: Helse ***Risk:***

Assessed consequence: **Small (1)**

Comment: [Ingen registreringer]

Overview of risk mitiating actions which have been decided:

Below is an overview of risk mitigating actions, which are intended to contribute towards minimizing the likelihood and/or consequence of incidents:

Overview of risk mitigating actions which have been decided, with description:

Detailed view of assessed risk for each hazard/incident before and after mitigating actions